Nuclear Inst. and Methods in Physics Research, A 1047 (2023) 167894

Contents lists available at ScienceDirect

Nuclear Inst. and Methods in Physics Research, A

journal homepage: www.elsevier.com/locate/nima

Neutron capture measurements with high efficiency detectors and the Pulse Height Weighting Technique

E. Mendoza [a,*], V. Alcayne [a], D. Cano-Ott [a], E. González-Romero [a], T. Martínez [a], A. Pérez de Rada [a], A. Sánchez-Caballero [a], J. Balibrea-Correa [b], C. Domingo-Pardo [b], J. Lerendegui-Marco [b], F. Calviño [c], C. Guerrero [d]

[a] Centro de Investigaciones Energéticas Medioambientales y Tecnológicas (CIEMAT), Spain
[b] Instituto de Física Corpuscular, CSIC - Universidad de Valencia, Spain
[c] Universitat Politècnica de Catalunya, Spain
[d] Universidad de Sevilla, Spain

ARTICLE INFO

Keywords:
Neutron capture
Total energy detector
Pulse height weighting technique
γ-ray cascades

ABSTRACT

Neutron capture cross section measurements in time-of-flight facilities are usually performed by detecting the prompt γ-rays emitted in the capture reactions. One of the difficulties to be addressed in these measurements is that the emitted γ-rays may change with the neutron energy, and therefore also the detection efficiency. To deal with this situation, many measurements use the so called Total Energy Detection (TED) technique, usually in combination with the Pulse Height Weighting Technique (PHWT). With it, it is sought that the detection efficiency depends only on the total energy of the γ-ray cascade, which does not vary much with the neutron energy. This technique was developed in the 1960s and has been used in many neutron capture experiments to date. One of the requirements of the technique is that γ-ray detectors have a low efficiency. This has meant that the PHWT has been used with experimental setups with low detection efficiencies. However, this condition does not have to be fulfilled by the experimental system as a whole. The main goal of this work is to show that it is possible to measure with a high efficiency detection system that uses the PHWT, and how to analyze the measured data.

1. Introduction

To measure neutron capture cross sections as a function of energy, time-of-flight facilities are commonly used [1–5]. A sample containing the isotope to be measured is placed in the neutron beam, and γ-ray detectors are usually located around the sample to detect the γ-rays resulting from the neutron capture reactions. The neutron beam has a pulsed structure so that the energy of the neutrons producing the capture reactions is determined from the detection time (time-of-flight).

There are several experimental limitations when performing time-of-flight neutron capture measurements [6]. Some of them are listed below:

1. Low counting statistics [7].
2. Large counting rates in the detectors, which may induce pile-up [8] and/or gain shifts as a function of the time-of-flight [9].
3. The so called γ-flash [10], which consists of ionizing radiation (γ-rays and other particles), which reaches the experimental area together with the neutron beam at short time-of-flights.
4. Background subtraction due to:
   (a) Sample activity [11].
   (b) Competing reaction channels: elastic scattering [12], inelastic [13], fission [14], ...
   (c) Background induced by the neutron beam [15].
   (d) In-beam γ-rays [16].
5. Angular dependence of the emitted γ-rays [16].
6. Sample related limitations: purity [17], inhomogeneities [18] ...

Some of these difficulties may be overcome with a suitable time-of-flight facility, a suitable sample and/or a suitable experimental setup. Regarding the experimental setup, some helpful features for these limitations are: having a large detection efficiency (limitation 1), using small and fast detectors (2 and 3), placing the detectors as close to the sample as possible (1, 4b and 4c), use background rejection capabilities (4a, 4b, 4c and 4d), use detectors with small sensitivity to competing reaction channels (4b), and placing the detectors at some selected angles, preferably at several different ones (4d and 5).

* Correspondence to: CIEMAT, Complutense 40, 28040 Madrid, Spain.
E-mail address: emilio.mendoza@ciemat.es (E. Mendoza).

[1] There may be also a direct reaction process contribution, but the compound-nucleus capture dominates in most practical cases.

https://doi.org/10.1016/j.nima.2022.167894
Received 28 September 2022; Received in revised form 17 November 2022; Accepted 28 November 2022
Available online 8 December 2022

In addition, one of the difficulties that must be taken into account when making this type of measurements is that the detection efficiency may change with the neutron energy. In a neutron capture reaction, the neutron is usually[1] absorbed by the target nucleus, creating then a nucleus with one more neutron which is in an excited state (compound nucleus [19,20]). This nucleus then decays to a state of lower energy (normally the ground state) emitting an electromagnetic cascade consisting mainly of γ-rays. The deexcitation pattern of this capture γ-ray cascade may change with the neutron energy, specially from one cross section resonance to other, since they correspond to different excited states of the compound nucleus.

One of the most widely used methods to overcome this difficulty is the Total Energy Detection (TED) technique [21], in which the efficiency of the detection system is intended to be proportional to the total energy of the (n, γ) cascade, and therefore does not depend on the deexcitation pattern. This technique, usually in combination with the so called Pulse Height Weighting Technique (PHWT) [22], described in the next section, has been extensively used during the last 60 years to measure many neutron capture cross sections [23–27].

Traditionally, the PHWT has been used with experimental setups with low detection efficiencies. This is a condition that has to be met for each of the individual detectors of the setup, but, in reality, does not have to be fulfilled by the experimental system as a whole. The main purpose of this work is to show that it is possible to build a high efficiency detection system which uses the PHWT. Such a detection system may have great advantages in measurements with low counting statistics. Another advantage is that the results of the measurement will not be strongly affected by a possible angular dependence of the emitted γ-rays, due to the high detection efficiency.

In this paper, we describe the PHWT with some detail in Section 2. There we first explain the technique when measuring with only one detector, to later extend it to the case of several detectors. After that, we show how to estimate the uncertainties due to counting statistics in the different cases.

In the next section, Section 3, we show the results of a large amount of Monte Carlo simulations intended to quantify how the (n, γ) detection efficiency change with the neutron energy, for a large variety of target nuclei. We have considered three different detection setups, with a low, an intermediate, and a large detection efficiencies. The simulated data have been analyzed with and without using the PHWT, in order to check the performance of the technique for realistic cascades.

Although it is not the main purpose of this work, we have taken advantage of this methodology to carry out a very similar study with the n_TOF Total Absorption Calorimeter (TAC) [28], which does not use the PHWT. The results of this study are shown in Section 4. Finally, the summary and conclusions of all this work are presented in Section 5.

2. The PHWT technique

2.1. The PHWT when measuring with one detector

The TED technique for one detector can be described in the following way. Let us assume that we use a γ-ray detector to detect (n, γ) cascades which fulfills the following conditions:

(i) The γ-ray detection efficiency (ε_γ) is low, i.e. $\varepsilon_\gamma \ll 1$, so that at most one γ-ray per cascade is detected.
(ii) The γ-ray detection efficiency is proportional to the energy of the γ-ray (E_γ): $\varepsilon_\gamma(E_\gamma) = k \cdot E_\gamma$.
(iii) The γ-rays of the cascades are emitted isotropically and without significative angular correlations.

Condition (ii) is achieved only by very specific detectors, or by applying the PHWT to the data collected by conventional γ-ray detectors, as will be seen later. Under these three conditions, the efficiency of detecting a particular capture cascade (ε_c), i.e. with a certain deexcitation pattern, is proportional to the total energy of the cascade (E_c):

$$\varepsilon_c = 1 - \prod_{i=1}^{n}(1 - \varepsilon_\gamma(E_{\gamma,i})) \simeq \sum_{i=1}^{n} \varepsilon_\gamma(E_{\gamma,i}) = k \cdot \sum_{i=1}^{n} E_{\gamma,i} = k \cdot E_c \quad (1)$$

In this expression the i index loops through the n γ-rays of the cascade. Since there are quite a few types of efficiencies in this document, we show them all in Table 1 for ease of reading.

Table 1
Description of the different efficiencies used in this document. In parenthesis, the first equation where the variable appears.

Symbol	Name and description
ε_γ	γ-ray detection efficiency: probability of detecting a γ-ray emitted by the source (Eq. (1)).
ε_c	Probability of detecting a particular capture cascade, i.e. with a specific deexcitation pattern (Eq. (1)).
ϵ_c	Capture detection efficiency: probability of detecting a neutron capture reaction (Eq. (5)).
ξ_c	Average number of pulses recorded by a detection system per capture reaction (Eq. (11)). In a detector system with multiple detectors, ξ_c is the sum of the capture detection efficiencies (ϵ_c) of the individual detectors.
ε_γ^w	Weighted γ-ray detection efficiency: similar to ε_γ, but when using the PHWT (Eq. (2)).
ε_c^w	Weighted cascade detection efficiency: similar to ε_c, but when using the PHWT (Eq. (4)).
ϵ_c^w	Weighted capture detection efficiency: similar to ϵ_c, but when using the PHWT (Eq. (6)).
ξ_c^w	Total weighted capture detection efficiency: similar to ξ_c, but when using the PHWT (Eq. (12)).

The efficiency of detecting a neutron capture reaction (ϵ_c, hereinafter called *capture detection efficiency*) will be the (weighted) average of the efficiencies of detecting all possible cascades, $\epsilon_c = \langle\varepsilon_c\rangle$, but since ε_c does not depend on the deexcitation pattern, we have that $\epsilon_c = \langle\varepsilon_c\rangle = k \cdot E_c$. The total energy of the cascade is very often nearly constant, since $E_c \simeq S_n + E_n$, where S_n is the neutron separation energy of the compound nucleus (typically ~5–10 MeV) and E_n the neutron energy, with $E_n \ll S_n$ in most cases. In all of the above we are assuming that the contribution of electrons and positrons to the total energy of the cascade is small.

The first measurements performed with the TED technique were performed with Moxon-Rae detectors [21,29], with a γ-ray detection efficiency which increases nearly linearly with γ-ray energy, i.e. fulfilling condition (ii). Later, it was seen that it was also possible to use this technique with detectors that did not fulfill condition (ii). To do this, it is enough to multiply each detected count by a weight, which depends on the energy deposited in the detector. By performing this operation, the proportionality condition can be recovered. This is usually called the Pulse Height Weighting Technique (PHWT) [22], and the main idea is to perform via *software* a similar operation than the one performed via *hardware* by the Moxon-Rae detectors.

In the beginning, measurements using the PHWT were performed using C_6F_6 detectors, but they were then usually replaced by C_6D_6 detectors [30,31], with smaller neutron sensitivity. Organic scintillators are used as well [25,32].

With the PHWT it is necessary to calculate the so called Weighting Function (WF or $W(E_d)$), which is a function of the energy deposited in the detector (E_d), and depends not only on the detector but also on the experimental setup [33]. The WF is computed to fulfill the following condition, which also defines the *weighted γ-ray detection efficiency* (ε_γ^w):

$$\varepsilon_\gamma^w(E_\gamma) = \int_0^\infty R(E_d, E_\gamma) W(E_d) dE_d = \kappa \cdot E_\gamma \quad (2)$$

where κ is a constant and $R(E_d, E_\gamma)$ is the response function of the detector, defined so that $\int_a^b R(E_d, E_\gamma) dE_d$ is the average number of pulses in the detector with deposited energies between $E_d = a$ and

$E_d = b$ per emitted γ-ray with energy E_γ. The γ-ray detection efficiency of the detector is then:

$$\varepsilon_\gamma(E_\gamma) = \int_0^\infty R(E_d, E_\gamma) d E_d \tag{3}$$

where the effect of the detection threshold is included in $R(E_d, E_\gamma)$.

The response functions were obtained initially from Monte Carlo simulations [22,34]. Some years later, discrepancies with results obtained from transmission experiments were found, and the origin of these discrepancies were attributed to problems related with the simulations [35]. An alternative method to obtain them experimentally was then developed [35,36], and used in several neutron capture cross section measurements. However, the fact that the response functions depend not only on the detector but also on the full experimental setup, including the sample which is being measured, limits the precision with which the response functions can be obtained experimentally. In addition, Monte Carlo simulation codes have improved significantly over time. For these reasons, the Monte Carlo method has been considered again the most accurate since some years ago [33,37].

In Eq. (2) κ plays the same role as k in Eq. (1). Both are constant values. However, we have decided to use different symbols to emphasize that k is a constant of the detection system, while κ can be set to any arbitrary value. The role of ε_γ^w is very similar to that of ε_γ. However, ε_γ^w is not a real efficiency and its value is not restricted to the interval [0,1], but will depend on the value of κ chosen.

Similarly to ε_c, we define a *weighted cascade detection efficiency* (ε_c^w):

$$\varepsilon_c^w = \sum_{i=1}^{n} \varepsilon_\gamma^w(E_{\gamma,i}) = \kappa \cdot \sum_{i=1}^{n} E_{\gamma,i} = \kappa \cdot E_c \tag{4}$$

where, again, we have assumed that at most one γ-ray per cascade is detected. In the previous expression ε_c^w refers to a particular deexcitation pattern with $i = 1, \ldots, n$ γ-rays.

In a neutron capture experiment $\epsilon_c = \langle \varepsilon_c \rangle$ can be used to estimate the number of capture reactions (N_c) from the number of pulses registered in the detector (C):

$$\hat{N}_c = \frac{C}{\epsilon_c} \tag{5}$$

where the hat indicates that $\hat{N}_c$ is an estimator of N_c. When using the PHWT, the *weighted capture detection efficiency* $\epsilon_c^w = \langle \varepsilon_c^w \rangle$ is used in a very similar way as ϵ_c to estimate N_c:

$$\hat{N}_c = \frac{\sum_i W(E_{d,i})}{\epsilon_c^w} = \frac{\sum_i W(E_{d,i})}{\kappa \cdot E_c} \tag{6}$$

where $\sum_i W(E_{d,i})$ is the sum of all the weights of the pulses registered in the detector.

In order to verify that Eq. (6) can be used to estimate the number of capture reactions that have taken place, we calculate the expected value ($E[\ ]$) of $\hat{N}_c$:

$$E\left[\hat{N}_c\right] = E\left[\frac{\sum_i W(E_{d,i})}{\epsilon_c^w}\right] = \frac{1}{\epsilon_c^w} E\left[\sum_i W(E_{d,i})\right] \tag{7}$$

where the i index loops over all the pulses registered in the detector.

For each γ-ray emitted in the (n, γ) reactions with energy E_γ, there will be a probability density function $f_{E_\gamma}(E_d)$ which describes the probabilities of depositing one energy or another in the detector. The expected value of the weight $W(E_d)$ corresponding to that γ-ray is then:

$$E\left[W(E_d)\right] = \int_0^\infty f_{E_\gamma}(E_d) W(E_d) d E_d \tag{8}$$

On the other hand, we have that $f_{E_\gamma}(E_d)$ is the probability of not detecting the γ-ray plus the response function $R(E_d, E_\gamma)$ of the detector. Taking this into account, it follows from Eqs. (2) and (8) that $E\left[W(E_d)\right] = \varepsilon_\gamma^w(E_\gamma)$. Therefore, the expected value of the sum of weights corresponding to a single capture reaction will be:

$$E\left[\sum_j W(E_{d,j})\right] = E\left[\sum_j \varepsilon_\gamma^w(E_{\gamma,j})\right] = E\left[\varepsilon_c^w\right] = \epsilon_c^w \tag{9}$$

where the j index loops over the γ-rays emitted in the capture reaction.

The expected value of the sum of all the weights of the pulses registered in the detector after N_c capture reactions (Eq. (7)) will be then:

$$E\left[\sum_i W(E_{d,i})\right] = N_c \epsilon_c^w \tag{10}$$

and therefore $E\left[\hat{N}_c\right] = N_c$.

2.2. The PHWT when measuring with various detectors

In the description given above it is assumed at all times that the measurements are made with a single detector. In practice, however, the experiments are usually performed with various detectors, typically between 2 and 4. In that case, the methodology can be correctly applied to each of the detectors separately, but it is less obvious how to combine the results obtained by each of them.

In most publications describing measurements using the PHWT, this topic is not mentioned. In the few that are done [9,22,38], what is stated is that when two or more pulses are detected in coincidence, then some of them are eliminated to avoid double counting. The effect of this operation in the final result can be taken into account by means of Monte Carlo calculations [9]. In any case, this effect is quite small in most cases, when the overall detection efficiency is small.

However, the TED technique (with or without the PHWT), can also be used with several detectors, even when there is a high total capture detection efficiency. The condition that has to be fulfilled is that each of the individual detectors is a TED. Namely, each individual detector must itself give a correct estimate of the number of capture reactions.

To estimate the number of capture reactions when measuring with various detectors and without using the PHWT, we can use the average number of pulses in our detection system per capture reaction (ξ_c) in a similar way as the capture detection efficiency (ϵ_c) is used in Eq. (5). If our system has m detectors, and conditions (i), (ii) and (iii) are fulfilled, then we will have that:

$$\xi_c = \sum_{j=1}^{m} \epsilon_{c,j} = \sum_{j=1}^{m} \langle \varepsilon_{c,j} \rangle = \sum_{j=1}^{m} \langle k_j \cdot E_c \rangle = \left(\sum_{j=1}^{m} k_j\right) \cdot E_c = \tilde{k} \cdot E_c \tag{11}$$

where $j = 1, \ldots, m$ loops through the m detectors, in each of them the capture detection efficiency is $\epsilon_{c,j} = k_j \cdot E_c$, and $\tilde{k} = \sum_{j=1}^{m} k_j$.

In a similar way, we can define when measuring with the PHWT a *total weighted capture detection efficiency* (ξ_c^w) as the sum of the weighted capture detection efficiencies:

$$\xi_c^w = \sum_{j=1}^{m} \epsilon_{c,j}^w = \sum_{j=1}^{m} (\kappa_j \cdot E_c) = \left(\sum_{j=1}^{m} \kappa_j\right) \cdot E_c = \tilde{\kappa} \cdot E_c \tag{12}$$

Each detector in the experimental setup will have its own weighting function, $W_j(E_d)$, and $\tilde{\kappa} = \sum_{j=1}^{m} \kappa_j$.

In a similar way to the one-detector case (Eqs. (5) and (6)), the number of capture reactions N_c when measuring with various detectors can be estimated as:

$$\hat{N}_c = \frac{\sum_{j=1}^{m} C_j}{\xi_c} = \frac{\sum_{j=1}^{m} C_j}{\tilde{k} \cdot E_c} \tag{13}$$

$$\hat{N}_c = \frac{\sum_{i,j} W_j(E_{d,i,j})}{\xi_c^w} = \frac{\sum_{i,j} W_j(E_{d,i,j})}{\tilde{\kappa} \cdot E_c} \tag{14}$$

where here C_j is the total number of pulses registered during our experiment in detector j, so $\sum_{j=1}^{m} C_j$ is the total number of pulses in all the detectors; and $\sum_{i,j} W_j(E_{d,i,j})$ is the sum of all the weights of the pulses registered in all the detectors. The first part of Eq. (13), $\hat{N}_c = \frac{\sum_{j=1}^{m} C_j}{\xi_c}$, is also valid when the TED technique is not used.

In fact, in the case of measuring with several detectors and not using the TED technique, the number of capture reactions can be estimated with both Eqs. (5) and (13). In the first case we will treat the entire detection system as if it were a single detector, and C will correspond to the number of events detected in coincidence. In the second case, we will add all the pulses registered in all the detectors, and then divide by ξ_c. Deciding which of the two methods is more convenient will depend not only on how fast each one converges, but also on the capture to background ratio obtained in each of the cases.

The explanation of Eq. (13) is clear, and the one for Eq. (14) can be performed using the same procedure as for Eq. (6). In both Eq. (13) and (14), what is being done is to average the results obtained in each of the individual detectors, weighing each result by the corresponding capture detection efficiency ($\epsilon_{c,j}$ or $\epsilon^{w}_{c,j}$). If the number of capture reactions estimated by each individual detector is correct (starting hypothesis), then the average (any average) will also lead to the correct value. What is, in principle, less obvious, is to decide which average is best to choose, and how to calculate the uncertainties due to counting statistics.

The question of the uncertainties is dealt with in the next subsection. Regarding which average is best to choose, the way the average is calculated when using the PHWT is determined by the values of κ_j. When there is only one detector, the value of κ has no impact in the final result. The same goes for the value of $\tilde{\kappa}$. However, the relative values between the different κ_j do have an impact. If $\hat{N}_{c,j}$ is the number of capture reactions estimated by detector j, so $\hat{N}_{c,j} = \frac{\sum_i W(E_{d,i,j})}{\epsilon^{w}_{c,j}}$, then Eq. (14) can be rewritten as:

$$\hat{N}_c = \frac{1}{\sum_j \epsilon^{w}_{c,j}} \sum_j \epsilon^{w}_{c,j} \cdot \hat{N}_{c,j} \tag{15}$$

Therefore, the $\epsilon^{w}_{c,j}$ values play the same role as the weights in a weighted average. In consequence, if, for example, all the κ_j are set to the same value (very often they are set to 1 MeV^{-1}, so $\epsilon^{w}_{c,j}$ have a value close to the neutron separation energy of the compound nucleus, in MeV) then $\hat{N}_c$ will be an unweighted average of the $\hat{N}_{c,j}$ values. This is probably a good choice, in general, if the uncertainties due to counting statistics are similar in all the detectors. This is the case, for example, when the response functions to the detected capture cascades are similar.

On the contrary, if the variation in the uncertainty values from one detector to another is large, then setting all κ_j to the same value will not be a good choice. If this is the case, one possibility is to compute first the uncertainties due to counting statistics of all $\hat{N}_{c,j}$ values, $\sigma_{s,j}$, and then set $\kappa_j \propto 1/\sigma^2_j$. This leads to $\hat{N}_c$ being calculated as a weighted mean of the $\hat{N}_{c,j}$ values. Other possibility would be to set $\kappa_j \propto \epsilon_{c,j}$, specially if the shape of the response functions of the detectors are similar. Both possibilities will be quite reasonable in most of the cases. To find the *best* κ_j one can always try to find those values which minimize the uncertainty in $\hat{N}_c$, which will depend not only on the values of σ_j, but also on the correlations (coincidences) between the detected pulses.

2.3. Uncertainties due to counting statistics

In experiments or in Monte Carlo calculations, the uncertainty due to counting statistics σ_s of a certain variable is usually determined in one of the following ways, depending if the form of the PDF that the variable is expected to follow is know or not:

1. If the form of the PDF is known, then this information can be used to estimate σ_s. For example, if the variable is expected to follow a Poisson distribution, then σ_s can be estimated as the square root of the estimated mean.
2. If the form of the PDF is not known, then the data (measured or computed) can be used to estimate it.

In the second case, all the data can be divided into N independent subsets with a similar size. In each of these subsets there will be an estimate x_i of the variable to be measured or computed, x, which is independent of the rest. The x_i values are expected to follow a PDF with unknown mean μ and unknown variance σ^2, which can be estimated from the sample values (x_i) with [39–41]:

$$\hat{\mu} = \langle x \rangle = \frac{1}{N} \sum_{i=1}^{N} x_i \tag{16}$$

$$\widehat{\sigma^2} = \frac{1}{N-1} \sum_{i=1}^{N} (x_i - \langle x \rangle)^2 \simeq \langle x^2 \rangle - \langle x \rangle^2 \tag{17}$$

where the $\simeq$ symbol is because $N-1$ has been replaced by N.

The value of $\hat{\mu}$ will be an estimate of the value which is being measured or computed. The uncertainty due to counting statistics can be then estimated as the standard deviation of $\hat{\mu}$. Since the variance of $\hat{\mu}$ is σ^2/N, we have that:

$$\sigma_s = \sigma_{\hat{\mu}} \simeq \frac{\sqrt{\langle x^2 \rangle - \langle x \rangle^2}}{\sqrt{N}} \tag{18}$$

This is the technique used to estimate the uncertainties due to counting statistics in standard Monte Carlo codes, such as MCNP [42]. There it is assumed that, for every Monte Carlo history (every time a new source is sampled), an independent measurement of x_i is being performed. Thus, N is the total number of histories calculated in the simulation. In the case of a time-of-flight experiment, a very similar approach can be performed, considering each neutron pulse as an independent measurement. If the intensity of the pulses fluctuates enough to introduce some bias, it is always possible to normalize the x_i values to the pulse intensity.

Another possibility to estimate the uncertainties due to counting statistics is to use a known form of the PDF. In the case of a time-of-flight experiment, the number of capture reactions in a certain time-of-flight interval are usually expected to follow a Poisson distribution. As a consequence, the number of capture reactions detected (both by one detector and by the whole detection system) will also follow a Poisson distribution. In Monte Carlo calculations, the binomial distribution can be used in some cases instead.

In the case at hand, we are interested in computing the uncertainty due to counting statistics in $\hat{N}_c$ obtained from the previous expressions, i.e. the uncertainties in C (Eq. (5)), $\sum_i W(E_{d,i})$ (Eq. (6)), $\sum_{j=1}^{m} C_j$ (Eq. (13)) and $\sum_{i,j} W_j(E_{d,i,j})$ (Eq. (14)).

Since in time-of-flight experiments C is assumed to follow a Poisson distribution, the uncertainty can be estimated as [41]:

$$\sigma_s(C) = \sqrt{C} \tag{19}$$

and the uncertainty in $\sum_i W(E_{d,i})$ as:

$$\sigma_s\left(\sum_i W(E_{d,i})\right) = \sqrt{\sum_i (W(E_{d,i}))^2}. \tag{20}$$

The last expression can be easily understood in the following way. Let us imagine that the weights, instead of being a continuous variable, could only adopt a finite number of discrete values. In this case we could always regroup the weights in the sum so that $\sum_i W(E_{d,i}) = \sum_{k=1}^{n_k} n_k \cdot W_k$, where $W_1, W_2, \ldots, W_{n_k}$ are the possible weight values and n_k is the number of times that W_k appears in the sum. Since the n_k values are expected to follow a Poisson distribution, we have that:

$$\begin{aligned} &\sigma^2_s\left(\sum_i W(E_{d,i})\right) = \sigma^2_s\left(\sum_k n_k \cdot W_k\right) = \\ &= \sum_k \sigma^2_s(n_k \cdot W_k) = \sum_k \left(n_k \cdot W^2_k\right) = \sum_i W^2_i \end{aligned} \tag{21}$$

which leads to Eq. (20). The case where $W(E_d)$ is a continuous variable corresponds to a limiting case of the discrete case, where $n_k \to \infty$.

For multiple detectors, if the number of capture reactions follows a Poisson distribution then the number of pulses registered in each individual detector and the number of detections in coincidence follows a Poisson distribution, but not the sum of pulses (or weights) of all the detectors. As a consequence, if the measurement is performed with the detectors in coincidence, then the uncertainties due to counting statistics in Eqs. (13) and (14) can be estimated with:

$$\sigma_s\left(\sum_{j=1}^{m} C_j\right) = \sqrt{\sum_k (c_k)^2} \tag{22}$$

where the k index loops over all the coincidences and c_k is the detection multiplicity of each event in coincidence (number of detectors that have registered a pulse in coincidence). And:

$$\sigma_s\left(\sum_{i,j} W_j\left(E_{d,i,j}\right)\right) = \sqrt{\sum_k \left(\sum_{k_1,k_2} W_{k_1}\left(E_{d,k_1,k_2}\right)\right)_k^2} \tag{23}$$

where, again, the k index loops over all the coincidences and $\sum_{k_1,k_2} W_{k_1}\left(E_{d,k_1,k_2}\right)$ is the sum of the weights of the pulses registered in each coincidence. Both Eqs. (22) and (23) can be deduced using a similar procedure that the one provided for Eq. (20).

In summary, Eqs. (19)–(23) can be used to estimate the uncertainties due to counting statistics in neutron capture experiments. If, for some reason, they cannot be used, for example if coincidences cannot be made, then Eq. (18) can be used instead. The only exception is probably when the shape of the PDF is very different from a Gaussian. In that case, the uncertainty would not be well determined by a standard deviation (of any kind), so other methods would have to be used, such as giving the estimated form of the PDF or providing additional information of some kind.

In Monte Carlo simulations, the obtained results are not expected to follow a Poisson distribution. Consequently, Eqs. (19)–(23) cannot be used, in general, to compute the uncertainty due to counting statistics. In this case, Eq. (18) should be used instead, or expressions derived from the binomial distribution equivalent to Eqs. (19)–(23), if the results are expected to follow a binomial distribution.

3. Monte Carlo calculations

Monte Carlo simulations play a very important role in the PHWT for two reasons. First, to calculate the weighting functions; and second, to correct for different effects (detection thresholds, electron conversion, etc.). When these corrections are made with sufficient precision, the uncertainties achieved in the cross sections due to the measurement technique has been estimated at 2% [33,37].

We have performed several Monte Carlo simulations in order to estimate how the detection of capture cascades may change with the neutron energy, i.e. from one cross section resonance to other, and also to test the performance of the PHWT in realistic conditions.

3.1. Geometry and data analysis

The simulations have been carried out with three different detection systems, all of them based on C_6D_6 detectors, which have been chosen to have a small (~5%–10%), intermediate (~15%–30%), and large (~50%–80%) capture detection efficiencies:

1. C6D6-01: A cylindrical C_6D_6 detector with 5 cm radius and 10 cm length (0.8 l volume), surrounded by 1 mm aluminum, located at 5 cm from the source.
2. C6D6-02: Two cylindrical C_6D_6 detectors with 5 cm radius and 13 cm length each (1.0 l each, 2.0 l in total), surrounded by 1 mm aluminum. They have been placed one in front of the other, separated by 6 cm. The source has been placed in the middle between them, at 3 cm from each detector.

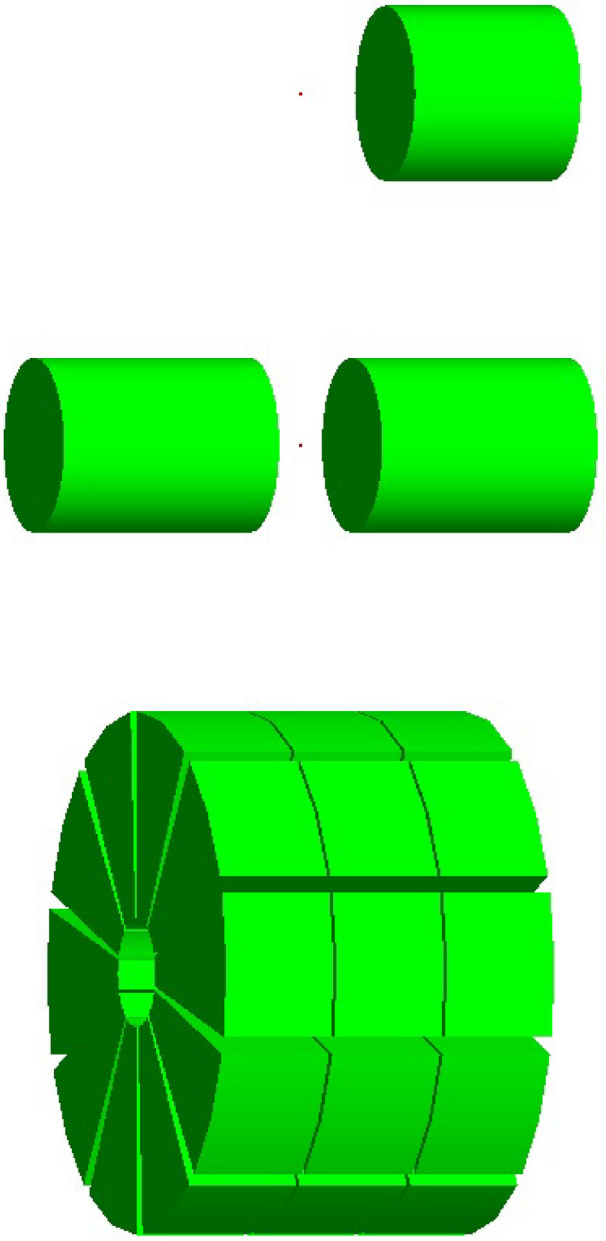

Fig. 1. Geometries used in the simulations for the C6D6-01 (top), C6D6-02 (middle) and slice-TED-01 (bottom) detectors.

3. slice-TED-01: a cylindrical C_6D_6 detector with 3 cm inner radius, 15 cm outer radius and 20 cm length. It has been segmented in 30 detectors, with 3 *slices* and 10 detectors per slice (13 l in total). Each of the 30 detectors is surrounded by 1 mm aluminum and the source is emitted from the center of the geometry.

A schematic view of the three detection systems are presented in Fig. 1.

The γ-rays and electrons emitted in the (n, γ) cascades have been emitted isotropically, without any angular correlation between them, from the center of a 1 mm radius aluminum sphere. They have been transported with Geant4 [43,44] to calculate the detector responses. The energy resolution of each C_6D_6, in terms of the Full Width Half Maximum (FWHM), has been modeled according to the following expression:

$$\frac{FWHM}{E_d} = \sqrt{a + \frac{b}{E_d}} \tag{24}$$

with $a = 0.0020$ and $b = 0.0083$ MeV [9].

The WFs of all the detectors have been calculated before simulating the cascades. For this, simulations of monoenergetic γ-rays of the three detection systems have been performed to obtain the response function of each individual detector, which has been used to compute the WFs in a similar way as in many other works [9,33,38]. It has been assumed that each WF (W_j) can be represented by a degree four polynomial, $W_j = \sum_{k=0}^{4} a_k \cdot E_d^k$. Thus, for each WF, the five a_k parameters have been fitted to minimize FOM_j, defined as:

$$FOM_j = \sum_{i=0}^{N_\gamma} \left(\kappa_j \cdot E_{\gamma,i} - \sum_{l=0}^{N_d} W_{j,l} \cdot R_{j,i,l} \right)^2 \quad (25)$$

where $R_{j,i,l}$ is the response matrix for detector j, which is a discretization of the response function $R_j(E_d, E_\gamma)$ in E_d and E_γ. The i index loops over the simulated γ-ray energies (N_γ in total), the l index loops over the deposited energy bins (N_d in total), and the j index refers to the detector. We have set all $\kappa_j = 1 MeV^{-1}$, so $\tilde{\kappa}$ will be equal to the number of detectors of the detection system, in MeV^{-1} units. This choice, in the case of slice-TED-01, has been made under the hypothesis that the differences between the detection efficiencies of the individual detectors are not very large (see the last part of Section 2.2).

3.2. Generation of the capture cascades: NuDEX

To simulate the capture cascades we have used NuDEX [45,46], which is a code which follows the same methodology as DICEBOX [47] or DEGEN [48]. To simulate the deexcitation process, NuDEX generates the full level scheme and branching ratios of the compound nucleus, taking all the values experimentally known from the RIPL-3 database [49], which takes the data from ENSDF [50]. The rest of the values are generated randomly according to statistical models. One of the main advantages of NuDEX is that it uses a database which allows it to generate capture cascades for a large amount of nuclei (~300), without requiring a specific input for each particular isotope.

The nuclear levels not present in the databases are generated randomly according to level densities, taken from RIPL-3. The distance between consecutive levels are sampled according to a Wigner distribution. The missing internal conversion coefficients are taken from [51].

The branching ratios not present in the databases are also generated randomly, according to the so called *extreme statistical model* [47]. The branching ratio of the transition from a level a to a level b, $BR_{a\to b}$, is computed according to:

$$BR_{a\to b} \propto \sum_{X,L} \xi_{a\to b}^2 E_\gamma^{2L+1} PSF^{XL}(E_\gamma, E_a) \quad (26)$$

where E_γ is the difference between the energy of the level a, E_a, and the energy of the level b, E_b; $\xi_{a\to b}$ is a random variable drawn independently from a normal distribution with zero mean and unit variance, which introduce the Porter-Thomas fluctuations; X is the type of transition (electric or magnetic); L is the multipolarity; and PSF^{XL} are the Photon Strength Functions (PSFs), which are taken from [52] and from RIPL-3.

Since part of the levels and branching ratios (in many cases most of them) are generated randomly, there is a very large number of possible sets of levels and branching ratios coming from the same level densities and PSFs. Each set will correspond to a specific random number string used (indeed, the number of possible sets is not *infinite* because the numbers in a computer have a limited precision). In this context, a *nuclear realization* [47] refers to one of these particular set of levels and branching ratios. The deexcitation pattern is then expected to vary from one realization to other, specially for nuclei with a small amount of levels. In addition, the deexcitation pattern will also depend, in general, on the level from which the cascade starts.

We have performed simulations with a large amount of nuclei. In order to simulate the effect of detecting capture cascades coming from different cross section resonances, i.e. levels of the compound nucleus, we have created several *subrealizations* [53] of the same realization. All the subrealizations of the same realization have the same levels and branching ratios with the exception of the branching ratios of the level where the cascade starts. Therefore, the cascades coming from each subrealization correspond to cascades coming from different cross section resonances. The spin and parity of each subrealization have been generated randomly, with a 50% probability for spins corresponding to s-wave resonances and 50% to p-wave. For each type of resonance, s or p, the spin has been sampled uniformly among all possible values.

The starting level to generate the cascade has been located 1 keV above the neutron separation energy of the compound nucleus. In each simulation, we have calculated the capture detection efficiency of the whole detection system, ϵ_c, and the total weighted capture detection efficiency, ξ_c^w. The uncertainties due to counting statistics have been obtained using Eq. (18). An energy threshold of 150 keV has been considered for each individual detector. For each subrealization, we have simulated 10^6 neutron capture cascades for the C6D6-01, $4 \cdot 10^5$ cascades for the C6D6-02, and 10^5 cascades for the slice-TED-01 detection systems. These quantities have been chosen to reach uncertainties due to counting statistics in ϵ_c and ξ_c^w below 1% in virtually all cases.

3.3. Results

An example of the obtained results is presented in Fig. 2. We have performed, for each of the three detection systems, 10^3 different simulations of the detection of ^{27}Al(n, γ) cascades. In each simulation, a different subrealization of the ^{28}Al nucleus has been generated. Namely, the (n, γ) cascades in each simulation corresponds to a different resonance. Fig. 2 shows the distribution of the obtained ϵ_c and ξ_c^w values.

Panel (a), for example, shows that the capture detection efficiency (ϵ_c) of the C6D6-01 detection systems (one C_6D_6 detector of 0.8 l located at 5 cm from the origin of the cascades) varies from 2% to 6%, approximately, depending on the subrealization considered. We have computed the standard deviation of the 10^3 obtained efficiencies (σ_r), obtaining $\sigma_r = 19\%$. This value can be used to quantify how the capture detection efficiency varies from one resonance to other, i.e. with the neutron energy, according to the predictions of the (n, γ) cascade generation model we are using. In this case, this variation is *large* because ^{28}Al is a light nucleus with a small number of levels, so changes in the primary transition probabilities induce significant changes in the deexcitation pattern.

The capture detection efficiencies for the C6D6-02 (two C_6D_6 detectors of 1 l each located at 3 cm from the origin of the cascades) and slice-TED-01 (30 detectors with 13 l in total at 3 cm from the origin of the cascades) detection systems are shown in panels (c) and (e). The obtained values are larger, as expected, and show a similar dispersion, $\sigma_r = 19\%$ and $\sigma_r = 15\%$, respectively.

The variations in ϵ_c and ξ_c^w are expected to come not only from variations in the deexcitation pattern, but also from statistical fluctuations due to the limited amount of histories run in the simulations. In order to estimate this contribution, the average uncertainty due to counting statistics (σ_s) is shown in each panel together with σ_r. Each σ_s value has been computed by performing an unweighted average of the 10^3 uncertainties due to counting statistics of the ϵ_c or ξ_c^w values. We can assume, in good approximation, that σ_r is the quadratic sum of two terms. One of them corresponds to the variations in the deexcitation pattern, and the other is σ_s.

When the PHWT is applied, the parameter which is equivalent to the capture detection efficiency is ξ_c^w, the total weighted capture detection efficiency. Since we have constructed the weighting functions so $\kappa_j = 1 MeV^{-1}$, ξ_c^w is expected to have a value close to the total energy of the cascade, in MeV, multiplied by the number of detectors of the setup. In this case the total energy of the cascade is very close to the neutron separation energy of ^{28}Al, which is $S_n(^{28}Al)$=7.7 MeV.

The distribution of the obtained ξ_c^w values for the three detection systems are presented at the bottom panels of Fig. 2. As expected,

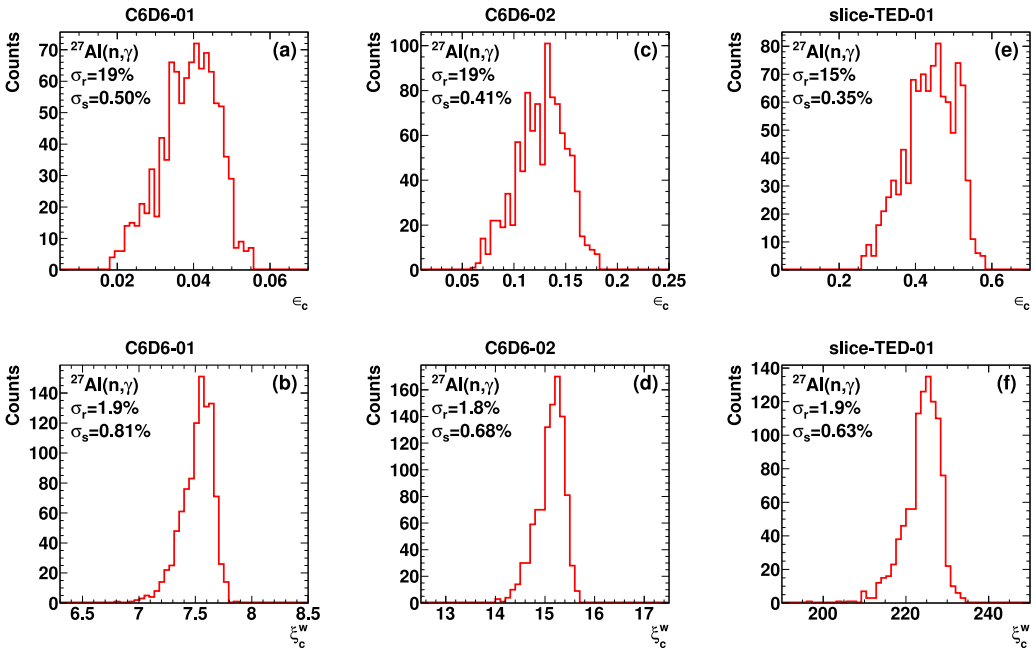

Fig. 2. Distribution of the capture detection efficiencies (ϵ_c, on the top panels) and the total weighted capture detection efficiencies (ξ_c^w, on the bottom panels) obtained from 10^3 different subrealizations of the ^{28}Al nucleus, used to model the ^{27}Al(n, γ) cascades. Three different experimental setups have been considered: C6D6-01 (left), C6D6-02 (middle) and slice-TED-01 (right). The standard deviation (σ_r) of the 10^3 obtained values is shown for each case, together with the unweighted average (σ_s) of the uncertainties due to counting statistics.

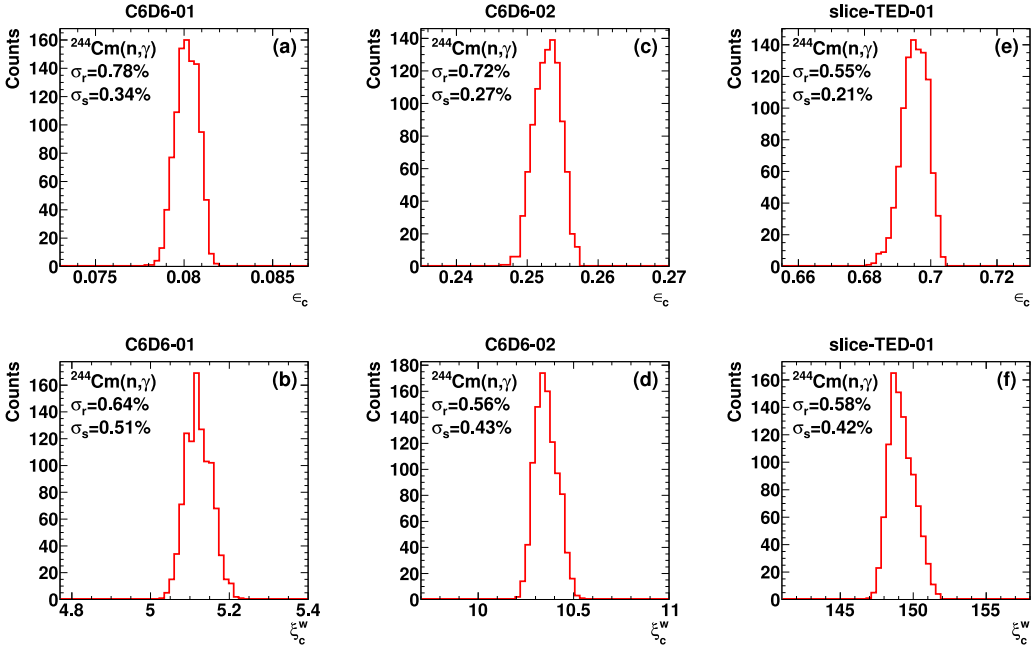

Fig. 3. Same as Fig. 2, but for ^{244}Cm(n, γ) cascades.

the width of the distributions decrease significantly. The standard deviations are now σ_r = 1.9% (C6D6-01), σ_r = 1.8% (C6D6-02) and σ_r = 1.9% (slice-TED-01), which indicates that the technique works quite well in all three cases.

The same type of calculations, but for ^{244}Cm(n, γ) cascades instead of ^{27}Al(n, γ), are presented in Fig. 3. Now the deexcitation pattern is expected to vary much less from one subrealization to other (and also from one realization to other). The reason is the much larger number of levels below the level from which the cascade starts ($\sim$ 200 for ^{27}Al(n, γ) vs $\sim 4 \cdot 10^6$ for ^{244}Cm(n, γ)). As expected, the standard deviations of the ϵ_c and ξ_c^w distributions are much smaller, below 1% in all three cases.

Therefore, according to the cascade generation model we are using, there are nuclei for which it is essential to use the PHWT, and others for which it is not really necessary. We will deal with this topic in more depth later, in Section 3.5.

Taking advantage of NuDEX's ability to generate capture cascades from a wide variety of nuclei, we have extended the simulations presented for ^{27}Al and ^{244}Cm to a list of about 200 nuclei. The simulations have been performed using the three detection systems presented

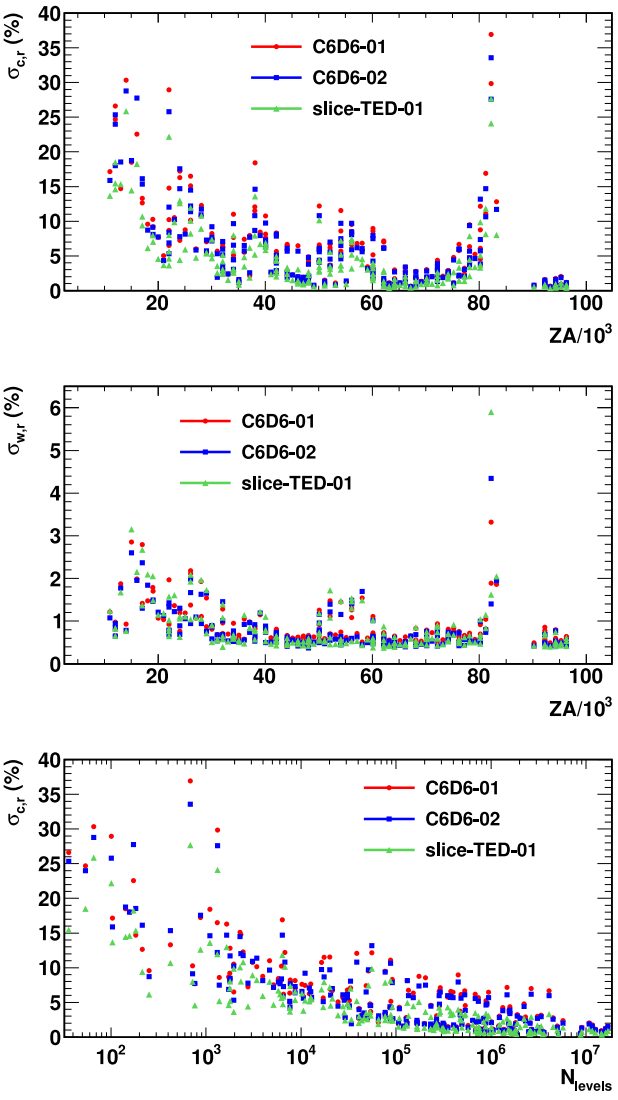

Fig. 4. The panels on the top and on the center, respectively, show the values of $\sigma_{c,r}$ and $\sigma_{w,r}$ from Table 3 (variations of ϵ_c and ξ_c^w with the neutron energy), as a function of the isotope. The isotope is defined as ZA=1000 ·Z+A, where Z and A are the atomic and mass numbers, respectively. The panel on the bottom shows the same $\sigma_{c,r}$ values as the panel on the top, but as a function of the number of levels in the compound nucleus below the level where the cascade starts (N_{levels}).

above. For each detection system and for each nuclei, 100 subrealizations have been simulated (instead of 10^3), with 10^6 (C6D6-01), $4 \cdot 10^5$ (C6D6-02) and 10^5 (slice-TED-01) cascades per simulation. The obtained results are summarized in Table 3, where it is shown, for each nuclei and detection system:

- The average capture detection efficiency, $\langle \epsilon_c \rangle$, obtained by performing an unweighted average of the 100 different ϵ_c values.
- The standard deviation of the 100 different ϵ_c values, $\sigma_{c,r}$.
- The unweighted average of the uncertainty due to counting statistics of the 100 different ϵ_c values, $\sigma_{c,s}$.
- The standard deviation of the 100 different ξ_c^w values, $\sigma_{w,r}$.
- The unweighted average of the uncertainty due to counting statistics of the 100 different ξ_c^w values, $\sigma_{w,s}$.

The values in Table 3 are intended to quantify the expected variations in ϵ_c and ξ_c^w as a function of neutron energy, for each nucleus and detection system. They show that the PHWT works quite well for virtually all the cases. In order to have a general overview of the values in Table 3, we present in Fig. 4 all the $\sigma_{c,r}$ and $\sigma_{w,r}$ values as a function of the isotope (top and center panels, respectively). The isotope is defined as ZA=1000 ·Z+A, where Z and A are the atomic and mass numbers, respectively. Fig. 4 shows that, according to the cascade generation model we are using, the detection efficiency are expected to vary by up to 30% (one standard deviation) from one cross section resonance to other, depending on the nucleus. On the contrary, when the PHWT is applied, then the variations are reduced below 2% in almost all the cases.

The panel on the bottom in Fig. 4 shows the same $\sigma_{c,r}$ values than the panel on the top, but as a function of the number of levels (N_{levels}) below the level where the cascade starts. As expected, there is a strong correlation between $\sigma_{c,r}$ and N_{levels}. The larger the number of levels, the smaller the dependence of the deexcitation pattern on the starting level, and therefore the smaller the variations in the detection efficiency.

The $\sigma_{c,s}$ and $\sigma_{w,s}$ values are presented in Table 3 to quantify the contribution of the statistical fluctuations originated by the limited number of simulated (n, γ) cascades in $\sigma_{c,r}$ and $\sigma_{c,s}$.

3.4. Counting statistics with the PHWT

In this section we study the effect of using weights in the statistical fluctuations when performing measurements with the PHWT. For this, we have carried out simulations with the same three detection systems as in the previous sections. In all cases, we have considered that the number of capture reactions that have taken place are expected to follow a Poisson distribution. Consequently, the uncertainties due to counting statistics have been estimated using Eqs. (19)–(23).

When the detection system is treated as a single detector and the PHWT is not used, the number of capture reactions can be estimated using Eq. (5), and the uncertainty due to counting statistics with Eq. (19). Hence:

$$\sigma_s\left(\hat{N}_c\right) = \sqrt{\frac{\hat{N}_c}{\epsilon_c}} \tag{27}$$

$$\frac{\sigma_s\left(\hat{N}_c\right)}{\hat{N}_c} = \frac{1}{\sqrt{N_{det}}} \tag{28}$$

where N_{det} is the number of capture events detected, denoted in the previous sections as C.

As a consequence, in this case capture detection efficiency and counting statistics are fully related. For example, to reduce the uncertainties due to counting statistics by a factor of two, a detection system with four times more efficiency is needed (Eq. (27)), provided that the same amount of capture events are being measured. The uncertainty due to counting statistics depends on the number of capture events detected only, and not in the way those events have been detected.

On the contrary, when using the PHWT the uncertainty due to counting statistics depends not only on the number of capture events detected, but also on how those events have been detected (deposited energies, detection multiplicities, etc.). It cannot be determined from the capture detection efficiency.

As an example, we show in Fig. 5 the evolution of the uncertainty due to counting statistics (σ_s) with the number of capture events detected for four different situations. All of them have been obtained from simulations of the detection of ^{65}Cu(n, γ) cascades with the C6D6-01 detection system, using the same nuclear realization. When the PHWT is not used (without WF) then $\sigma_s(\%) = 100/\sqrt{N_{det}}$, and σ_s depends only on N_{det}. The other three curves (with WF) correspond to the evolution of σ_s when using the PHWT, in three different simulations. Despite having simulated in the three cases cascades coming from the same nucleus, the evolution of σ_s with N_{det} is different in each case, since they depend on the specific energies deposited in the detector. The more different the weights that contribute to the sums in Eqs. (6) and (6), the larger the uncertainty.

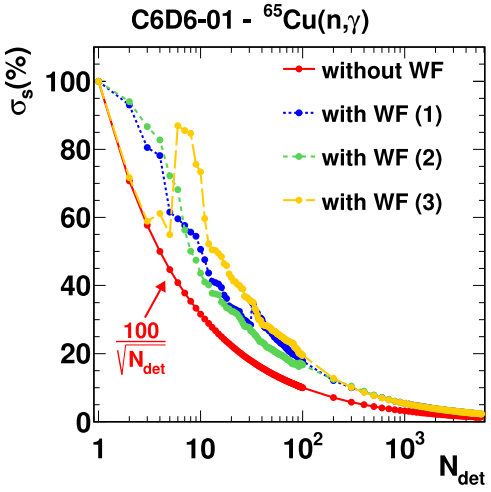

Fig. 5. Uncertainties due to counting statistics (σ_s) in $\hat{N}_c$ as a function of the number of capture events detected (N_{det}), obtained in simulations performed with the C6D6-01 detection system when detecting ^{65}Cu(n, γ) cascades. Four different results are presented. One of them (without WF) corresponds to the evolution of the uncertainty when the PHWT is not used. The other three (with WF) correspond to different simulations using the PHWT, all of them using the same nuclear realization.

In order to study in more detail the evolution of σ_s with N_{det} when using the PHWT, we have extended the number of simulations to 1000 instead of three. The mean value, standard deviation and minimum and maximum σ_s values of the 1000 different results have been computed at each N_{det} value, and the obtained results are presented in Fig. 6.

The uncertainties when using the PHWT are always equal or larger than when it is not. This is a consequence of Eqs. (5), (6), (19) and (20). Fig. 6 also shows that the differences between the σ_s values obtained in the different simulations increase with N_{det} when N_{det} is small, and decrease with N_{det} when N_{det} is large.

In this particular case, the ratio between the σ_s values obtained with the PHWT ($\sigma_{s,w}$) and the σ_s value obtained when the PHWT is not used ($\sigma_{s,c}$) converges to ~1.7 when N_{det} becomes large. According to Eq. (27), measuring with a detector with $1.7 \times 1.7 \simeq 3$ times smaller capture detection efficiency and not using the PHWT would lead to uncertainties due to counting statistics similar to $\sigma_{s,w}$. Thus, in this case using the PHWT has an effect on the statistical fluctuations equivalent to reducing the capture detection efficiency by a factor of ~3, for large N_{det}. For small values of N_{det}, such a comparison makes less sense.

For the next step, we have performed the same type of comparison, but now using cascades from different nuclei. Specifically, we have carried out 100 simulations of each of the ~ 200 nuclei that appear in Table 3. Each simulation has been performed using (n, γ) cascades coming from a different nuclear subrealization. We have then computed the mean value, standard deviation, etc., of the ~ 20.000 obtained results, and these values have been divided by $\sigma_{s,c}$, as in the right panel of Fig. 6. The results are shown in Fig. 7, for the three detection systems considered in this work.

Contrary to Fig. 6, the ratios do not converge to a specific value as N_{det} increases. This is because for each capture cascade the ratio converges to a different value. It does seem that above ~ 100 captures detected, the ratios do not vary much. In order to be able to observe to what values these ratios converge, and also to compare the different detection systems, we show in Fig. 8 the distributions of the ~ 20.000 $\sigma_{s,w}/\sigma_{s,c}$ values for large N_{det}. The three distributions have been obtained for $N_{det} = 10^4$, but for any N_{det} above $N_{det} \simeq 10^3$ very similar values are obtained, since they have already converged.

Fig. 8 shows that these ratios converge to values between 1.3 and 2, approximately. It also shows that the distributions are very similar for the C6D6-01 and C6D6-02 detection systems, but with the slice-TED-01 the ratios converge to smaller values. This means that with the slice-TED-01 not only more capture reactions will be detected, due to its larger efficiency, but also that when detecting the same number of capture reactions as with the other two detection systems, the uncertainties due to the counting statistics will be, in general, smaller. We attribute this effect to the increase in the number of pulses detected in coincidence, which increases the number of terms in the sum in Eq. (14) more than in Eq. (5).

Table 2
Number of nuclei in Table 3 with $\sigma_{c,r}$ smaller than the values in the first column. The total number of nuclei in Table 3 is 202.

$\sigma_{c,r}$ max.	C6D6–01	C6D6–02	slice-TED-01
1%	14	19	40
2%	58	62	77
3%	83	85	103
4%	96	98	130
5%	106	111	146

The effect of using weights on the statistical fluctuations can be considered, for large N_{det}, equivalent to using a detector with lower efficiency. Specifically, according to Eq. (27), with an efficiency ϵ_c^* which is $\epsilon_c^* = \sigma_{s,c}^2/\sigma_{s,w}^2 \times \epsilon_c$. In fact, we could define an *equivalent capture detection efficiency* ϵ_c^* in this way, which would serve to calculate the uncertainties due to counting statistics from the number of capture cascades detected when using the PHWT (for large N_{det}).

The distribution of $\sigma_{s,w}^2/\sigma_{s,c}^2$ ratios are then the same as ϵ_c/ϵ_c^*, and can be obtained from the distributions in Fig. 8 just by squaring the values on the X axis. Thus, the values of ϵ_c^* are $\sim 2-3.5$ times smaller than ϵ_c for the C6D6-01 and C6D6-02 detection systems, and $\sim 1.8-2.5$ times smaller for the slice-TED-01.

3.5. Measuring without the PHWT

The results of this work show that, according to the cascade generation model we are using, there are a large amount of nuclei where the detection efficiency does not change much with the neutron energy. Table 2 summarizes the number of nuclei which appear in Table 3 with a small value of $\sigma_{c,r}$. There it is shown that, for example, 29% (31%, 38%) of the simulated nuclei present a $\sigma_{c,r}$ smaller than 2% for the C6D6-01 (C6D6-02, slice-TED-01) setup. This allows to measure some nuclei without the PHWT, using experimental setups which usually apply the PHWT.

This has already been done, for example, in the ^{242}Pu(n, γ) cross section measurement performed recently at n_TOF [15,38] with four C_6D_6 detectors. In the data analysis, the capture yield was obtained both using the PHWT and without using it (named weighted and unweighted yields, respectively). Both yields were compared, and it was found that they were compatible within uncertainties. As expected, the statistical fluctuations in the unweighted yield were smaller, so the resonance analysis was performed with the unweighted yield, after normalizing it to the weighted yield. The same procedure was followed afterwards for the analysis of the ^{240}Pu and ^{244,246,248}Cm (n, γ) cross section measurements performed also at n_TOF [7,9]. Other example of a measurement performed with C_6D_6 detectors and which did not use the PHWT is a ^{237}Np(n, γ) measurement performed at the Research Reactor Institute, Kyoto University (KURRi) [54].

Having smaller statistical fluctuations is not the only advantage of measuring without the PHWT. Other advantage is that, in some circumstances, the capture to background ratio may be improved. This was the case of the ^{242}Pu(n, γ) measurement, as reported in [38]. There, the amplitude spectra in the detectors due to the ^{242}Pu(n, γ) cascades and due to the background had shapes such that the capture to background ratio was larger when the PHWT was not applied.

In addition, measuring without the PHWT allows to impose some conditions on the detected events to discriminate background events from capture events. This may substantially improve the results of

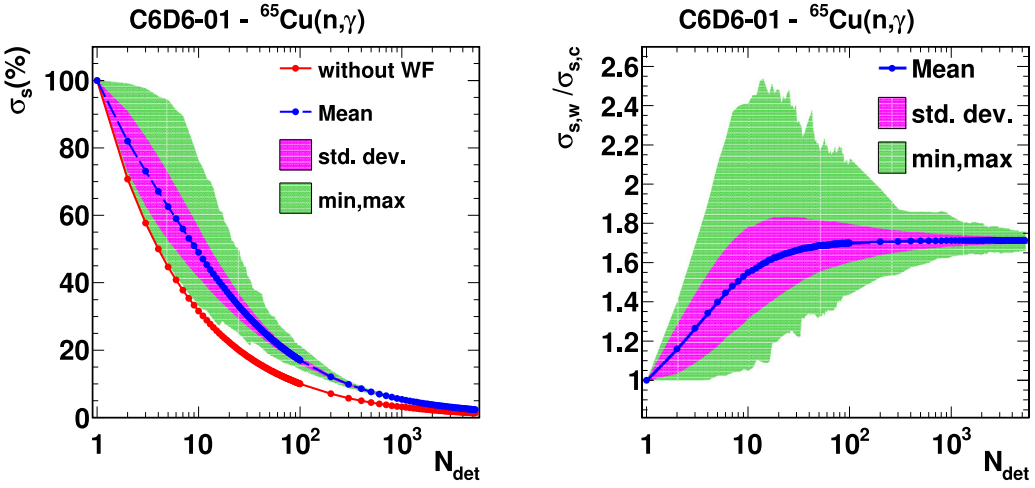

Fig. 6. Evolution of σ_s with N_{det} when performing the same type of simulations as in Fig. 5. On the left, the mean value (mean), standard deviation (std. dev.) and minimum and maximum (min,max) values obtained from 1000 different simulations performed using the PHWT are compared with the case of not using the PHWT (without WF). On the right, the same values but divided by the *without WF* case, i.e. the ratio between the uncertainties obtained when using the PHWT and when it is not.

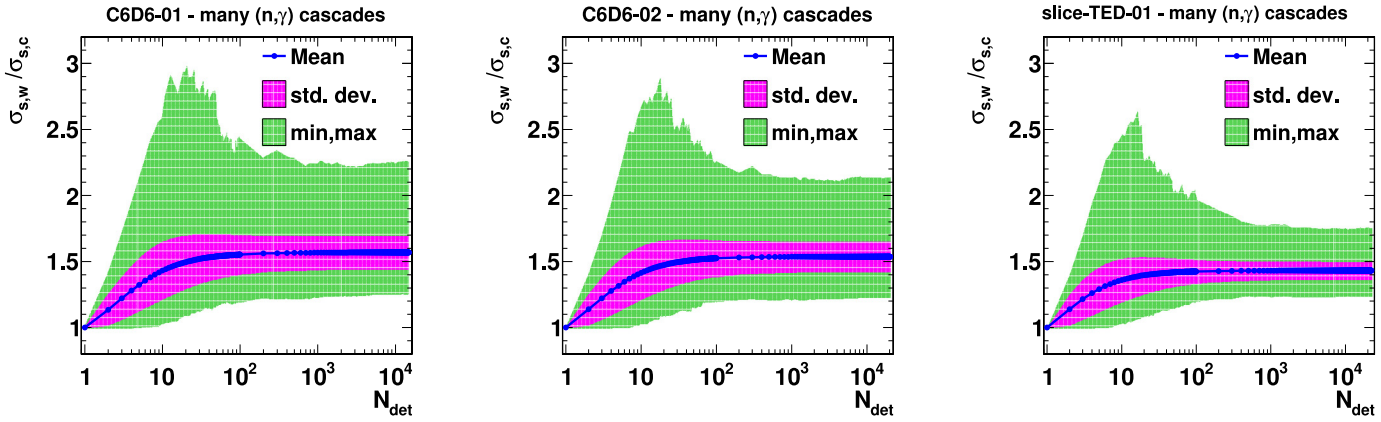

Fig. 7. Ratio between the uncertainties due to counting statistics obtained when analyzing the data using the PHWT and without using it, as a function of the number of capture reactions detected (N_{det}). The ratios have been obtained from simulations performed with ∼ 20.000 different (n, γ) cascades, coming from ∼ 200 different nuclei. What is shown is the mean, the standard deviation (std. dev.) and the minimum and maximum values (min,max) of the obtained ratios. The calculations have been performed using the three detection systems considered in this work: C6D6-01 (left), C6D6-02 (center) and slice-TED-01 (right).

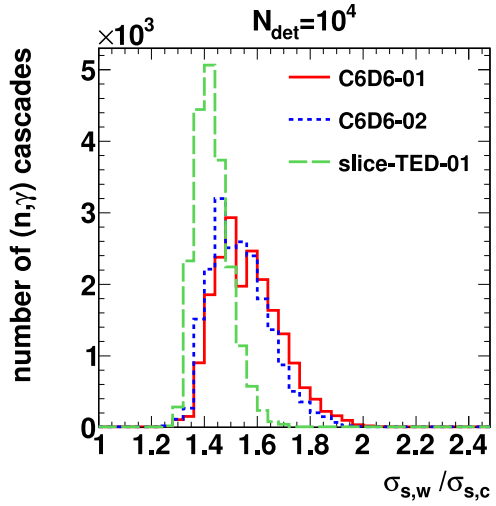

Fig. 8. Distributions of the same $\sigma_{s,w}/\sigma_{s,c}$ ratios used in Fig. 7, obtained after detecting 10^4 (n, γ) cascades.

the measurement in some cases, even at the cost of measuring with markedly smaller detection efficiency.

The PHWT does not allow, as far as we know, to discriminate some detected events from others, except in very specific cases. Some of these cases is when the detected events are clearly not from the reaction being measured. Or when they have a very low probability. For example, when the energy deposited in the detector is larger than that of the (n, γ) cascade.

In addition to conditions on the deposited energy, another possible condition is in the detection multiplicity. If the background in the experimental facility is dominated by events with multiplicity one (γ-rays coming from outside the experimental setup, for example) then it may be beneficial to exclude them from the data analysis. To do this, it is necessary that the probability of detecting (n, γ) cascades with a multiplicity larger than one do not be too low. This would be another advantage of measuring with a high-efficiency segmented detector.

As an example, we show in Fig. 9 the detection multiplicity distributions obtained in three simulations performed with the slice-TED-01. The three simulations correspond to (n, γ) cascades from ^{27}Al, ^{139}La and ^{244}Cm. For ^{244}Cm, which could be measured without using the PHWT, the detection efficiency of the slice-TED-01 is reduced to 30% if we exclude events with multiplicity one. In this case, measuring with this condition in multiplicities could be a very good choice if the capture to background ratio improves significantly.

Table 3
Summary of the results obtained after performing simulations of the detection of (n, γ) cascades with three different detection systems. For each nuclei and detection system, cascades from 100 different subrealizations of the compound nucleus have been modeled, emulating the differences in the deexcitation pattern from different cross section resonances. For each nuclei and detection system, we show the average value of the obtained detection efficiencies ($\langle\epsilon_c\rangle$), the standard deviation of the ϵ_c values ($\sigma_{c,r}$), the average of the uncertainties due to counting statistics in the ϵ_c values ($\sigma_{c,s}$), the standard deviation of the ξ_c^w values ($\sigma_{w,r}$), and the average of the uncertainties due to counting statistics in the ξ_c^w values ($\sigma_{w,s}$). All the values are given in per cent (%).

Iso	C6D6-01					C6D6-02					slice-TED-01				
	$\langle\epsilon_c\rangle$ (%)	$\sigma_{c,r}$ (%)	$\sigma_{c,s}$ (%)	$\sigma_{w,r}$ (%)	$\sigma_{w,s}$ (%)	$\langle\epsilon_c\rangle$ (%)	$\sigma_{c,r}$ (%)	$\sigma_{c,s}$ (%)	$\sigma_{w,r}$ (%)	$\sigma_{w,s}$ (%)	$\langle\epsilon_c\rangle$ (%)	$\sigma_{c,r}$ (%)	$\sigma_{c,s}$ (%)	$\sigma_{w,r}$ (%)	$\sigma_{w,s}$ (%)
^{23}Na	4.6	17	0.45	1.2	0.72	15	16	0.38	1.1	0.61	48	14	0.33	1.2	0.58
^{24}Mg	5.1	25	0.43	0.81	0.81	17	24	0.35	0.85	0.67	52	19	0.3	0.82	0.64
^{25}Mg	6.5	18	0.38	0.97	0.72	21	18	0.31	0.94	0.6	62	15	0.25	0.84	0.55
^{26}Mg	4.8	27	0.44	0.66	0.73	15	25	0.37	0.65	0.62	50	15	0.31	0.66	0.57
^{27}Al	4.2	15	0.48	1.9	0.78	13	19	0.4	1.8	0.67	44	15	0.35	1.7	0.62
^{28}Si	3.2	30	0.55	0.93	0.9	10	29	0.46	0.78	0.76	37	26	0.41	0.77	0.69
^{31}P	4.0	18	0.49	2.9	0.85	14	19	0.4	2.6	0.7	46	14	0.34	3.2	0.65
^{32}S	4.4	23	0.46	2.0	0.82	14	28	0.39	2.0	0.69	48	18	0.33	2.2	0.63
^{35}Cl	5.5	13	0.41	2.8	0.75	17	15	0.35	2.4	0.64	54	11	0.29	2.7	0.59
^{37}Cl	5.8	13	0.4	1.4	0.64	18	16	0.33	1.3	0.55	57	9.4	0.28	1.4	0.51
^{40}Ar	6.8	9.6	0.37	1.5	0.62	22	8.7	0.3	1.8	0.51	63	6.1	0.24	2.1	0.5
^{39}K	6.1	10	0.39	1.8	0.65	20	9.1	0.32	1.5	0.55	59	8.0	0.26	2.1	0.51
^{41}K	6.8	9.2	0.37	1.7	0.68	22	8.1	0.3	1.5	0.56	62	7.0	0.25	1.5	0.54
^{40}Ca	6.9	7.7	0.37	1.1	0.58	22	7.7	0.3	1.2	0.48	66	4.6	0.23	1.2	0.45
^{45}Sc	6.0	5.0	0.39	1.0	0.74	19	4.3	0.32	1.1	0.63	57	3.7	0.27	1.2	0.58
^{46}Ti	5.9	8.7	0.4	1.4	0.69	19	6.9	0.33	1.3	0.57	59	4.6	0.27	1.0	0.53
^{47}Ti	7.9	10	0.34	2.0	0.69	25	8.4	0.27	1.4	0.58	69	5.6	0.21	1.6	0.53
^{48}Ti	7.7	6.5	0.35	0.78	0.57	24	5.3	0.28	0.79	0.47	69	3.6	0.21	0.83	0.45
^{49}Ti	8.7	15	0.32	0.92	0.59	27	12	0.26	0.69	0.49	73	8.0	0.19	0.76	0.46
^{50}Ti	3.9	29	0.49	0.76	0.78	13	26	0.4	0.77	0.64	44	22	0.35	0.65	0.61
^{51}V	5.0	11	0.43	1.4	0.74	16	10	0.36	1.2	0.62	51	9.9	0.31	1.6	0.59
^{50}Cr	6.8	7.2	0.37	0.77	0.69	21	7.8	0.3	0.69	0.59	65	4.4	0.23	0.63	0.53
^{52}Cr	5.1	17	0.43	1.2	0.74	16	18	0.36	1.3	0.63	51	13	0.31	1.1	0.59
^{53}Cr	6.6	16	0.38	1.3	0.7	21	15	0.31	0.89	0.6	61	13	0.25	1.1	0.55
^{55}Mn	5.3	8.7	0.42	1.2	0.73	17	8.1	0.35	1.1	0.62	53	5.9	0.3	1.1	0.58
^{54}Fe	5.0	15	0.44	2.2	0.8	16	14	0.35	1.7	0.66	51	10	0.31	1.9	0.62
^{56}Fe	4.1	16	0.48	2.1	0.84	14	12	0.39	2.0	0.69	45	12	0.35	2.1	0.65
^{57}Fe	6.8	10	0.37	1.4	0.68	21	11	0.3	0.94	0.57	63	8.2	0.24	1.0	0.52
^{59}Co	5.6	6.0	0.41	1.1	0.71	18	5.8	0.33	1.1	0.6	56	4.7	0.28	1.1	0.56
^{58}Ni	5.2	11	0.43	1.9	0.8	17	11	0.35	1.6	0.68	53	8.9	0.3	2.0	0.62
^{60}Ni	4.6	12	0.45	1.1	0.78	15	12	0.37	0.94	0.65	49	11	0.32	1.1	0.61
^{63}Cu	5.8	5.3	0.4	0.87	0.72	19	5.7	0.33	0.76	0.59	57	5.5	0.28	0.72	0.56
^{65}Cu	5.9	7.0	0.4	1.5	0.69	19	7.3	0.33	1.7	0.58	57	5.4	0.27	1.7	0.55
^{64}Zn	5.1	7.4	0.43	0.81	0.69	16	9.2	0.36	0.59	0.58	54	5.3	0.29	0.51	0.53
^{66}Zn	5.5	8.2	0.41	0.9	0.67	18	7.7	0.34	0.89	0.57	54	7.4	0.29	0.91	0.54
^{68}Zn	6.6	7.5	0.38	0.9	0.63	21	7.2	0.31	0.87	0.53	62	4.7	0.25	0.9	0.5
^{69}Ga	7.6	5.7	0.35	0.69	0.62	24	5.3	0.28	0.68	0.52	67	3.6	0.22	0.58	0.5
^{71}Ga	6.4	2.0	0.38	0.68	0.62	21	1.9	0.31	0.54	0.52	61	2.5	0.25	0.55	0.5
^{70}Ge	7.2	3.1	0.36	0.63	0.62	23	3.5	0.29	0.68	0.52	64	2.8	0.24	0.65	0.5
^{72}Ge	7.0	2.9	0.36	0.71	0.62	22	2.8	0.29	0.57	0.51	64	2.4	0.24	0.57	0.49
^{73}Ge	12	6.8	0.27	0.57	0.51	35	6.0	0.21	0.62	0.43	83	3.1	0.14	0.4	0.41
^{74}Ge	5.2	6.3	0.43	1.3	0.69	17	7.1	0.35	1.5	0.59	52	5.1	0.3	1.4	0.56
^{76}Ge	6.7	6.3	0.37	0.96	0.63	21	5.1	0.3	1.0	0.53	62	4.2	0.25	1.1	0.51
^{75}As	6.5	2.3	0.38	0.7	0.63	21	2.4	0.31	0.54	0.53	61	1.6	0.25	0.53	0.5
^{76}Se	6.7	2.8	0.37	0.6	0.62	21	3.1	0.3	0.61	0.52	62	2.6	0.25	0.6	0.5
^{77}Se	9.0	4.6	0.32	0.62	0.57	28	4.4	0.26	0.52	0.48	73	2.9	0.19	0.59	0.45
^{78}Se	7.0	5.1	0.36	0.66	0.63	22	4.5	0.29	0.68	0.53	64	3.1	0.24	0.64	0.5
^{80}Se	6.3	7.6	0.39	0.75	0.66	20	6.5	0.31	0.58	0.54	60	5.8	0.26	0.65	0.52
^{82}Se	5.2	11	0.43	0.95	0.69	17	9.7	0.35	0.77	0.58	53	8.0	0.3	0.68	0.55
^{79}Br	8.0	1.2	0.34	0.67	0.6	25	1.1	0.27	0.52	0.51	69	0.86	0.21	0.51	0.48
^{81}Br	7.7	1.5	0.35	0.61	0.6	24	1.6	0.28	0.51	0.5	67	1.4	0.22	0.55	0.48
^{83}Kr	11	7.4	0.28	1.1	0.51	34	6.5	0.22	0.93	0.43	82	3.5	0.15	1.1	0.41
^{84}Kr	7.9	5.5	0.34	0.57	0.55	24	5.7	0.28	0.56	0.47	68	4.8	0.22	0.48	0.45
^{85}Rb	8.2	2.1	0.33	0.76	0.61	26	2.6	0.27	0.73	0.51	70	1.9	0.21	0.83	0.48
^{87}Rb	5.5	7.9	0.41	0.98	0.65	18	7.7	0.34	0.96	0.55	55	6.2	0.28	0.84	0.52
^{86}Sr	6.6	12	0.38	0.88	0.66	21	8.7	0.3	0.91	0.54	61	7.9	0.25	0.81	0.52
^{87}Sr	12	12	0.27	0.59	0.47	36	11	0.21	0.53	0.4	83	5.2	0.14	0.57	0.37
^{88}Sr	5.6	18	0.41	0.82	0.63	18	15	0.34	0.65	0.54	56	14	0.28	0.76	0.51
^{89}Y	5.9	8.4	0.4	1.1	0.63	19	7.9	0.33	1.2	0.53	58	6.7	0.27	1.2	0.5
^{90}Zr	6.2	6.2	0.39	0.79	0.58	20	7.3	0.32	0.88	0.49	60	5.9	0.26	0.8	0.47
^{91}Zr	9.3	11	0.31	0.5	0.56	28	9.7	0.25	0.5	0.47	74	6.9	0.19	0.53	0.45
^{92}Zr	6.0	7.6	0.39	0.76	0.64	19	6.6	0.32	0.74	0.53	59	6.3	0.27	1.1	0.51
^{94}Zr	6.3	8.1	0.39	0.84	0.58	20	6.4	0.31	0.77	0.48	61	5.2	0.25	0.75	0.46
^{93}Nb	7.3	2.6	0.36	0.61	0.6	23	2.7	0.29	0.51	0.5	65	2.4	0.23	0.47	0.48
^{92}Mo	6.8	5.6	0.37	0.6	0.58	21	5.1	0.3	0.5	0.49	64	3.7	0.24	0.43	0.46
^{94}Mo	6.5	5.3	0.38	0.63	0.62	21	4.5	0.31	0.58	0.52	61	4.4	0.25	0.54	0.5

(*continued on next page*)

Table 3 (*continued*).

Iso	C6D6-01					C6D6-02					slice-TED-01				
	$\langle\epsilon_c\rangle$ (%)	$\sigma_{c,r}$ (%)	$\sigma_{c,s}$ (%)	$\sigma_{w,r}$ (%)	$\sigma_{w,s}$ (%)	$\langle\epsilon_c\rangle$ (%)	$\sigma_{c,r}$ (%)	$\sigma_{c,s}$ (%)	$\sigma_{w,r}$ (%)	$\sigma_{w,s}$ (%)	$\langle\epsilon_c\rangle$ (%)	$\sigma_{c,r}$ (%)	$\sigma_{c,s}$ (%)	$\sigma_{w,r}$ (%)	$\sigma_{w,s}$ (%)
^{95}Mo	9.7	8.3	0.3	0.81	0.55	30	7.9	0.24	0.73	0.46	77	4.4	0.17	0.64	0.44
^{96}Mo	6.5	4.1	0.38	0.78	0.64	21	4.0	0.31	0.73	0.54	60	3.0	0.26	0.65	0.51
^{97}Mo	10	8.1	0.3	0.69	0.52	30	8.1	0.24	0.61	0.44	77	5.0	0.17	0.65	0.42
^{98}Mo	6.8	2.7	0.37	0.75	0.59	22	2.9	0.3	0.68	0.49	63	2.0	0.24	0.57	0.47
^{100}Mo	5.8	2.5	0.4	0.63	0.6	19	2.8	0.33	0.61	0.5	57	2.6	0.27	0.51	0.49
^{99}Ru	10	6.4	0.29	0.55	0.53	32	5.7	0.23	0.41	0.44	78	3.3	0.17	0.48	0.42
^{101}Ru	11	6.7	0.29	0.48	0.51	32	6.1	0.23	0.45	0.43	79	3.1	0.16	0.44	0.41
^{102}Ru	6.5	2.8	0.38	0.57	0.61	21	2.7	0.31	0.57	0.51	61	2.4	0.25	0.6	0.5
^{104}Ru	5.9	2.2	0.4	0.66	0.59	19	1.9	0.33	0.62	0.49	58	1.7	0.27	0.49	0.48
^{103}Rh	6.9	2.3	0.37	0.6	0.6	22	2.2	0.3	0.56	0.5	63	1.5	0.24	0.49	0.48
^{104}Pd	7.9	1.9	0.34	0.55	0.58	25	1.9	0.27	0.54	0.49	68	1.3	0.22	0.54	0.47
^{105}Pd	11	6.5	0.29	0.61	0.51	32	5.7	0.23	0.46	0.43	79	3.1	0.16	0.48	0.41
^{106}Pd	7.5	1.8	0.35	0.56	0.56	24	2.0	0.28	0.47	0.47	67	1.2	0.22	0.46	0.45
^{108}Pd	7.3	1.6	0.36	0.62	0.57	23	1.6	0.29	0.47	0.48	65	1.2	0.23	0.53	0.47
^{110}Pd	7.2	1.5	0.36	0.51	0.54	23	1.3	0.29	0.42	0.46	65	0.99	0.23	0.47	0.44
^{107}Ag	7.8	1.6	0.34	0.65	0.58	25	1.3	0.28	0.47	0.48	68	0.88	0.22	0.53	0.46
^{109}Ag	7.7	1.9	0.35	0.6	0.57	24	1.9	0.28	0.5	0.48	67	1.1	0.22	0.43	0.46
^{110}Cd	7.7	1.5	0.35	0.54	0.56	24	1.4	0.28	0.57	0.47	67	1.2	0.22	0.53	0.46
^{111}Cd	10	4.2	0.3	0.47	0.51	31	3.8	0.24	0.37	0.43	77	2.2	0.17	0.42	0.4
^{112}Cd	7.9	1.8	0.34	0.61	0.56	25	1.9	0.27	0.53	0.47	68	1.2	0.22	0.53	0.45
^{113}Cd	9.2	4.9	0.31	0.67	0.53	28	4.8	0.25	0.59	0.45	73	2.7	0.19	0.6	0.43
^{114}Cd	7.1	2.0	0.36	0.55	0.56	23	1.6	0.29	0.55	0.47	65	1.2	0.23	0.51	0.45
^{116}Cd	6.7	1.9	0.37	0.59	0.57	22	2.1	0.3	0.62	0.48	63	1.5	0.24	0.58	0.46
^{115}In	8.6	0.74	0.33	0.63	0.53	27	0.78	0.26	0.51	0.44	71	0.6	0.2	0.47	0.43
^{116}Sn	6.8	4.3	0.37	0.76	0.58	21	4.1	0.3	0.8	0.49	62	2.7	0.24	0.74	0.46
^{117}Sn	9.4	6.1	0.31	0.66	0.51	29	5.6	0.25	0.5	0.43	74	3.4	0.19	0.55	0.41
^{118}Sn	7.5	3.7	0.35	0.74	0.55	23	4.4	0.29	0.75	0.46	66	3.0	0.23	0.7	0.44
^{119}Sn	8.9	6.6	0.32	0.57	0.53	27	6.0	0.26	0.53	0.44	72	4.3	0.2	0.59	0.42
^{120}Sn	6.6	5.7	0.38	0.92	0.58	21	6.1	0.31	1.2	0.49	61	4.4	0.25	0.97	0.47
^{124}Sn	5.5	12	0.41	1.3	0.65	18	11	0.34	0.96	0.54	54	10	0.29	1.2	0.53
^{121}Sb	7.8	0.9	0.34	0.59	0.57	25	0.93	0.28	0.47	0.48	68	0.74	0.22	0.56	0.46
^{123}Sb	7.5	1.5	0.35	0.55	0.57	24	1.4	0.28	0.52	0.48	67	0.94	0.22	0.52	0.46
^{125}Te	9.3	6.2	0.31	0.56	0.52	29	5.6	0.25	0.55	0.44	74	3.5	0.19	0.46	0.42
^{126}Te	7.1	3.5	0.36	1.1	0.59	22	3.6	0.29	1.2	0.5	64	2.4	0.24	1.1	0.48
^{128}Te	6.9	3.7	0.37	0.71	0.58	22	4.5	0.3	0.68	0.49	63	3.1	0.24	0.62	0.47
^{130}Te	6.6	6.7	0.38	1.5	0.6	21	7.0	0.31	1.4	0.51	61	5.6	0.25	1.7	0.49
^{127}I	7.1	1.1	0.36	0.68	0.58	23	0.79	0.29	0.58	0.49	65	0.84	0.23	0.47	0.47
^{129}Xe	9.5	5.7	0.31	0.59	0.53	29	5.1	0.25	0.48	0.45	75	3.0	0.18	0.49	0.43
^{131}Xe	10	7.1	0.29	0.6	0.52	31	6.5	0.23	0.49	0.44	78	3.6	0.17	0.57	0.42
^{132}Xe	7.3	4.8	0.36	0.59	0.57	23	4.6	0.29	0.45	0.48	65	3.6	0.23	0.46	0.46
^{134}Xe	5.9	12	0.4	0.74	0.62	19	9.7	0.33	0.64	0.52	57	7.2	0.27	0.57	0.49
^{136}Xe	7.4	8.6	0.35	1.5	0.52	23	7.5	0.29	1.2	0.44	67	5.2	0.22	1.5	0.43
^{133}Cs	7.1	1.2	0.36	0.62	0.58	23	1.4	0.29	0.55	0.49	65	0.93	0.23	0.49	0.47
^{135}Ba	9.5	6.6	0.31	0.55	0.52	29	5.9	0.25	0.6	0.44	75	3.2	0.18	0.53	0.42
^{136}Ba	5.5	7.1	0.42	1.3	0.65	18	8.1	0.34	1.5	0.54	55	7.0	0.28	1.5	0.51
^{137}Ba	7.7	9.5	0.34	1.3	0.56	24	9.7	0.28	1.4	0.47	67	7.4	0.22	1.3	0.45
^{138}Ba	7.6	8.5	0.35	1.1	0.54	24	8.5	0.28	1.4	0.46	67	5.2	0.22	1.5	0.45
^{139}La	6.0	6.8	0.39	0.71	0.6	19	6.2	0.32	0.63	0.5	59	4.7	0.27	0.54	0.48
^{140}Ce	8.6	5.9	0.33	0.51	0.51	27	5.6	0.26	0.45	0.43	72	3.8	0.2	0.44	0.42
^{142}Ce	5.6	6.8	0.41	1.5	0.6	18	6.1	0.33	1.7	0.51	57	4.5	0.28	1.5	0.49
^{141}Pr	6.6	3.4	0.38	0.6	0.57	21	3.1	0.3	0.5	0.48	62	3.0	0.25	0.57	0.46
^{142}Nd	9.0	3.2	0.32	0.69	0.49	28	3.0	0.25	0.53	0.42	74	2.0	0.19	0.57	0.41
^{143}Nd	12	8.6	0.27	0.56	0.46	35	7.5	0.21	0.47	0.39	83	3.6	0.14	0.57	0.38
^{144}Nd	6.1	5.2	0.39	1.1	0.57	20	4.2	0.32	1.0	0.47	60	3.2	0.26	1.0	0.46
^{145}Nd	11	9.0	0.28	0.62	0.48	34	7.9	0.22	0.62	0.41	81	4.0	0.15	0.38	0.39
^{146}Nd	6.8	2.8	0.37	0.67	0.55	22	2.6	0.3	0.64	0.46	63	1.5	0.24	0.6	0.45
^{148}Nd	7.0	1.9	0.36	0.56	0.55	22	1.8	0.3	0.54	0.46	64	1.5	0.24	0.48	0.45
^{150}Nd	5.8	3.1	0.4	0.72	0.57	19	2.6	0.33	0.58	0.48	58	2.0	0.27	0.53	0.46
^{147}Sm	12	7.1	0.27	0.72	0.46	35	6.1	0.21	0.65	0.39	83	2.7	0.14	0.88	0.38
^{148}Sm	8.1	1.5	0.34	0.52	0.52	26	1.1	0.27	0.44	0.43	70	0.92	0.21	0.38	0.42
^{149}Sm	11	7.0	0.28	0.63	0.47	34	6.2	0.22	0.49	0.4	81	2.9	0.15	0.71	0.39
^{150}Sm	7.0	0.88	0.37	0.59	0.55	22	0.89	0.3	0.48	0.46	64	0.63	0.24	0.44	0.45
^{152}Sm	7.1	1.1	0.36	0.56	0.57	23	0.96	0.29	0.45	0.47	65	0.73	0.23	0.44	0.46
^{154}Sm	6.2	1.6	0.39	0.73	0.56	20	1.8	0.32	0.63	0.47	60	1.3	0.26	0.56	0.45
^{151}Eu	7.7	1.1	0.35	0.56	0.53	24	1.0	0.28	0.46	0.45	68	0.63	0.22	0.44	0.43
^{153}Eu	7.6	0.63	0.35	0.51	0.54	24	0.52	0.28	0.53	0.45	68	0.35	0.22	0.42	0.44
^{155}Gd	7.9	1.4	0.34	0.65	0.51	25	1.3	0.28	0.6	0.43	69	0.78	0.21	0.63	0.41
^{156}Gd	7.6	0.76	0.35	0.62	0.54	24	0.67	0.28	0.4	0.45	68	0.53	0.22	0.4	0.43
^{157}Gd	7.7	3.0	0.35	0.61	0.52	24	2.7	0.28	0.45	0.43	68	1.7	0.21	0.5	0.41
^{158}Gd	7.0	1.3	0.36	0.53	0.54	22	1.4	0.3	0.49	0.45	65	1.0	0.23	0.49	0.44
^{160}Gd	7.5	1.7	0.35	0.57	0.54	24	1.4	0.28	0.5	0.45	67	1.2	0.22	0.48	0.44
^{159}Tb	7.3	1.1	0.36	0.54	0.55	23	1.1	0.29	0.44	0.46	66	0.8	0.22	0.47	0.44
^{161}Dy	8.2	2.8	0.33	0.49	0.51	26	2.6	0.27	0.4	0.43	71	1.5	0.2	0.45	0.41

(*continued on next page*)

Table 3 (*continued*).

Iso	C6D6-01					C6D6-02					slice-TED-01				
	$\langle\epsilon_c\rangle$ (%)	$\sigma_{c,r}$ (%)	$\sigma_{c,s}$ (%)	$\sigma_{w,r}$ (%)	$\sigma_{w,s}$ (%)	$\langle\epsilon_c\rangle$ (%)	$\sigma_{c,r}$ (%)	$\sigma_{c,s}$ (%)	$\sigma_{w,r}$ (%)	$\sigma_{w,s}$ (%)	$\langle\epsilon_c\rangle$ (%)	$\sigma_{c,r}$ (%)	$\sigma_{c,s}$ (%)	$\sigma_{w,r}$ (%)	$\sigma_{w,s}$ (%)
^{162}Dy	7.9	1.3	0.34	0.54	0.56	25	1.0	0.27	0.5	0.46	68	0.66	0.22	0.43	0.45
^{163}Dy	7.8	3.4	0.34	0.5	0.52	25	3.4	0.28	0.51	0.44	69	2.0	0.21	0.48	0.42
^{164}Dy	6.8	1.9	0.37	0.63	0.56	22	1.7	0.3	0.47	0.47	63	1.1	0.24	0.47	0.46
^{165}Ho	7.5	0.65	0.35	0.65	0.54	24	0.55	0.28	0.65	0.45	67	0.44	0.22	0.59	0.44
^{166}Er	8.0	1.1	0.34	0.56	0.53	25	0.66	0.27	0.42	0.44	70	0.52	0.21	0.44	0.43
^{167}Er	8.0	2.8	0.34	0.83	0.51	25	2.7	0.27	0.68	0.43	70	1.4	0.21	0.85	0.42
^{168}Er	6.7	1.5	0.37	0.54	0.54	21	1.8	0.3	0.46	0.46	64	1.4	0.24	0.54	0.44
^{170}Er	6.9	1.8	0.37	0.5	0.54	22	2.0	0.3	0.41	0.45	64	1.3	0.23	0.47	0.44
^{169}Tm	7.3	1.4	0.36	0.53	0.55	23	1.2	0.29	0.46	0.46	66	0.94	0.23	0.48	0.44
^{171}Yb	7.8	1.6	0.34	0.52	0.5	25	1.4	0.28	0.42	0.42	69	0.97	0.21	0.45	0.41
^{172}Yb	7.6	1.2	0.35	0.64	0.54	24	1.1	0.28	0.51	0.46	68	0.97	0.22	0.58	0.44
^{173}Yb	7.2	3.0	0.36	0.65	0.51	23	2.8	0.29	0.47	0.43	66	1.8	0.23	0.6	0.41
^{174}Yb	7.3	1.4	0.36	0.8	0.55	23	1.3	0.29	0.76	0.46	66	1.3	0.23	0.75	0.45
^{176}Yb	7.1	2.0	0.36	0.74	0.56	23	1.9	0.29	0.65	0.47	65	1.4	0.23	0.66	0.45
^{175}Lu	7.6	2.1	0.35	0.73	0.53	24	2.0	0.28	0.53	0.44	68	0.97	0.22	0.6	0.43
^{176}Hf	9.3	1.3	0.31	0.52	0.51	29	1.3	0.25	0.42	0.43	75	0.76	0.18	0.43	0.42
^{177}Hf	8.2	3.2	0.33	0.94	0.49	26	3.0	0.27	0.74	0.41	71	1.6	0.2	0.87	0.4
^{178}Hf	7.1	1.9	0.36	0.87	0.55	23	2.1	0.29	0.77	0.46	65	1.6	0.23	0.74	0.44
^{179}Hf	8.1	4.4	0.34	0.84	0.51	25	3.9	0.27	0.72	0.43	70	2.1	0.21	0.9	0.41
^{180}Hf	6.0	3.7	0.4	0.7	0.55	19	3.2	0.32	0.66	0.46	59	2.6	0.26	0.59	0.45
^{181}Ta	7.4	2.1	0.35	0.56	0.54	23	1.9	0.29	0.46	0.45	66	1.1	0.22	0.46	0.43
^{182}W	6.7	2.7	0.37	0.6	0.55	21	2.7	0.3	0.53	0.46	63	2.2	0.24	0.56	0.45
^{183}W	7.4	2.9	0.35	0.81	0.53	23	2.3	0.29	0.74	0.44	66	1.7	0.23	0.7	0.43
^{184}W	6.5	2.4	0.38	0.66	0.55	21	2.4	0.31	0.57	0.46	62	1.8	0.25	0.52	0.45
^{186}W	6.3	2.9	0.38	0.72	0.56	20	2.7	0.31	0.61	0.47	61	2.4	0.26	0.71	0.46
^{185}Re	7.5	1.1	0.35	0.83	0.54	24	1.1	0.28	0.69	0.45	67	0.75	0.22	0.67	0.44
^{187}Re	7.2	4.8	0.36	0.76	0.54	23	4.4	0.29	0.71	0.46	65	2.6	0.23	0.92	0.44
^{188}Os	7.1	2.2	0.36	0.53	0.55	22	2.1	0.29	0.46	0.46	65	1.4	0.23	0.49	0.45
^{189}Os	8.4	6.7	0.33	0.76	0.51	26	6.0	0.26	0.72	0.43	71	3.3	0.2	0.58	0.41
^{190}Os	6.9	2.1	0.37	0.56	0.57	22	2.2	0.3	0.43	0.48	64	1.4	0.24	0.52	0.46
^{192}Os	5.9	5.8	0.4	0.63	0.57	19	6.0	0.33	0.5	0.48	58	4.3	0.27	0.54	0.47
^{191}Ir	7.5	2.3	0.35	0.65	0.56	24	2.0	0.28	0.43	0.47	67	1.4	0.22	0.45	0.45
^{193}Ir	7.0	3.2	0.37	0.66	0.57	22	3.0	0.3	0.57	0.48	64	2.0	0.24	0.62	0.46
^{194}Pt	6.4	4.5	0.38	0.59	0.61	20	4.7	0.31	0.52	0.51	60	3.4	0.26	0.52	0.49
^{195}Pt	9.0	3.9	0.32	0.62	0.53	28	3.7	0.26	0.55	0.45	72	2.1	0.2	0.51	0.43
^{196}Pt	6.0	6.3	0.4	0.65	0.61	19	5.7	0.32	0.54	0.52	59	4.5	0.27	0.66	0.5
^{198}Pt	5.3	9.5	0.42	0.72	0.64	17	9.4	0.35	0.6	0.54	53	7.9	0.29	0.52	0.52
^{197}Au	6.5	5.2	0.38	0.57	0.61	21	4.6	0.31	0.52	0.51	61	3.4	0.25	0.5	0.49
^{198}Hg	7.1	4.5	0.36	0.6	0.58	22	3.9	0.29	0.51	0.48	64	3.3	0.24	0.47	0.47
^{199}Hg	8.1	6.1	0.34	0.92	0.58	25	5.7	0.27	1.0	0.48	69	3.7	0.21	1.0	0.46
^{200}Hg	4.9	12	0.44	0.7	0.67	16	13	0.36	0.56	0.57	51	9.8	0.31	0.61	0.54
^{201}Hg	8.8	8.7	0.32	0.6	0.59	28	7.4	0.26	0.51	0.49	72	5.1	0.2	0.68	0.47
^{203}Tl	5.2	11	0.43	0.82	0.69	17	11	0.35	0.74	0.58	52	8.1	0.3	0.83	0.56
^{205}Tl	5.1	17	0.43	1.0	0.77	17	15	0.35	0.8	0.64	51	12	0.31	1.2	0.62
^{206}Pb	4.0	30	0.48	1.9	0.82	13	28	0.4	1.4	0.69	45	24	0.34	1.6	0.64
^{207}Pb	3.7	37	0.5	3.3	0.76	12	34	0.42	4.3	0.66	41	28	0.37	5.9	0.61
^{209}Bi	5.8	13	0.4	1.9	0.63	19	12	0.33	1.9	0.52	57	8.0	0.27	2.1	0.51
^{232}Th	7.4	0.76	0.35	0.49	0.51	24	0.78	0.28	0.42	0.42	67	0.58	0.22	0.42	0.41
^{233}U	8.7	1.6	0.32	0.57	0.47	27	1.5	0.26	0.48	0.39	73	0.88	0.19	0.46	0.38
^{235}U	9.0	1.2	0.32	0.78	0.46	28	1.2	0.25	0.68	0.38	74	0.64	0.19	0.72	0.37
^{236}U	7.7	0.82	0.35	0.53	0.5	24	0.8	0.28	0.49	0.42	69	0.63	0.21	0.41	0.41
^{238}U	6.3	1.1	0.39	0.86	0.51	20	0.95	0.31	0.69	0.43	61	0.72	0.25	0.66	0.42
^{237}Np	7.7	0.63	0.35	0.49	0.5	24	0.52	0.28	0.42	0.42	69	0.37	0.21	0.4	0.41
^{238}Pu	7.8	0.55	0.34	0.5	0.5	25	0.57	0.28	0.53	0.42	69	0.47	0.21	0.49	0.41
^{239}Pu	8.4	1.3	0.33	0.59	0.47	26	1.3	0.27	0.41	0.4	72	0.83	0.2	0.42	0.39
^{240}Pu	7.8	0.66	0.34	0.53	0.5	25	0.62	0.28	0.4	0.42	69	0.51	0.21	0.47	0.41
^{241}Pu	8.5	1.7	0.33	0.56	0.46	27	1.6	0.26	0.46	0.39	72	0.94	0.2	0.52	0.38
^{242}Pu	7.9	0.74	0.34	0.8	0.5	25	0.69	0.27	0.77	0.42	69	0.46	0.21	0.75	0.41
^{241}Am	7.7	0.92	0.35	0.52	0.5	24	0.77	0.28	0.49	0.42	68	0.55	0.22	0.43	0.41
^{243}Am	7.4	2.0	0.35	0.54	0.5	24	1.9	0.29	0.46	0.42	67	1.1	0.22	0.49	0.41
^{244}Cm	8.0	0.8	0.34	0.63	0.51	25	0.73	0.27	0.54	0.43	69	0.42	0.21	0.6	0.42
^{246}Cm	7.1	1.2	0.36	0.64	0.54	23	1.1	0.29	0.53	0.45	65	0.87	0.23	0.54	0.44
^{248}Cm	6.9	1.1	0.37	0.55	0.51	22	0.96	0.3	0.43	0.43	64	0.71	0.24	0.41	0.42

4. Neutron capture measurements with the n_TOF TAC

The TED technique is not the only one used to measure neutron capture cross sections in time-of-flight facilities. The first measurements were performed using very large liquid scintillator tanks [55], with a large detection efficiency. The idea of this method is to achieve an efficiency close to 100%, so that, as in the TED technique, the efficiency does not change significantly with the neutron energy. Later, high efficiency segmented detectors were built using inorganic materials such as NaI, BaF_2 or BGO. Some examples are the detectors at the Kurchatov Atomic Energy Institute [56] (NaI), at the Rensselaer Polytechnic Institute (RPI) [57] (NaI), at the FZK Karlsruhe [58] (BaF_2), and at the Research Reactor Institute of the Kyoto University [59] (BGO).

As explained in great detail in section 2 of [58], one of the main advantages of these detectors over the large liquid scintillator tanks is the larger total absorption efficiency and energy resolution. This allows, in principle, to impose some conditions on the detected events to discriminate a significant fraction of the measured background while

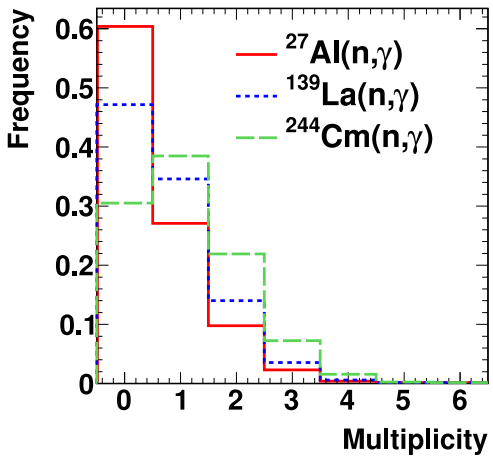

Fig. 9. Distribution of the detection multiplicities obtained in simulations carried out with the slice-TED-01 when detecting (n, γ) cascades from three different nuclei. In the three cases the results correspond to simulations preformed with a particular nuclear realization. The first bin on the left, centered at zero multiplicity, corresponds to the probability of not detecting the cascade, so the sum of the bin contents is in all cases 1.

keeping large detection efficiencies. In the BaF_2 Karlsruhe detector, for example, the conditions are chosen to keep the efficiencies above 90% [60,61]. This ensures that the efficiency depends very little on the individual γ-ray cascades.

Two BaF_2 detectors very similar to the one at the FZK Karlsruhe are the n_TOF TAC at CERN [28], with 40 crystals, and the DANCE detector at the Los Alamos Neutron Science Center [62], with 160 crystals. In addition, another detector very similar to the n_TOF TAC, named GTAF-II, has been recently built at the CSNS Back-n facility [63]. All of them have been designed to detect a large fraction of the γ-ray cascade energy. However, in practice most of the measurements have been performed with conditions on the detected events so that the capture detection efficiency becomes far from 100%. Some examples are the efficiencies in the ^{237}Np(n, γ) [64] (ϵ_c = 70%), ^{243}Am(n, γ) [65] (ϵ_c = 56%) and ^{241}Am(n, γ) [8] (ϵ_c = 37%) measurements performed with the n_TOF TAC; and the efficiencies in the ^{236}U(n, γ) [66] (ϵ_c = 16%), ^{241}Am(n, γ) [67] (ϵ_c = 12.5%) and ^{65}Cu(n, γ) [68] (ϵ_c = 45%) measurements performed with DANCE.

From the results we have presented in the previous section, this should not be a problem when measuring cross sections of actinides, since the efficiency is not expected to change from one resonance to another. Indeed, it has been verified experimentally in some cases (see for example Fig. 6 in [8]). However, it is not straightforward whether these detectors can be used to measure lighter isotopes. To date, only actinides have been measured with the n_TOF TAC, however, lighter isotopes have also been measured with DANCE.

This topic is addressed in [68] for the analysis of the ^{65}Cu(n, γ) measurement mentioned above. Several simulations were carried out with DICEBOX to estimate the variations in the detector efficiency with the neutron energy. The results they obtained were variations of 4.4%, not far from those obtained in this work and shown in Table 3 (5.4% for the slice-TED-01). Other similar work with DANCE can be found in [69].

In order to investigate the changes in the detection efficiency with the n_TOF TAC, we have carried out a study similar to the one shown in the previous section. For the same ~200 nuclei, we have generated with NuDEX 100 different subrealizations, with 10^6 cascades per simulation. The spin and parity of each subrealization have been generated as before, with 50% probability for s-wave and 50% for p-wave resonances. The cascades have been transported using the same Geant4 geometry as in previous works [70]. The results were reconstructed in the same way as in a real experiment, including the energy resolution of the detectors. An energy threshold of 150 keV has been applied to each BaF_2 crystal. The geometry included the same neutron absorber made of borated polyethylene used in the ^{241}Am(n, γ) measurement [8].

For each event detected in coincidence, some cuts on the total deposited energy (E_{sum}) and detection multiplicity (m_{cr}) are usually applied. For this study, we have selected events with $E_{sum} > 2.5$ MeV, since this is a cut used in all the measurements performed up to now, which tries to avoid the detection of the 2.2 MeV γ-ray emitted in ^{1}H(n, γ) reactions. Several cuts on m_{cr} have been considered. For each nuclei and cut on m_{cr}, the mean value $\langle\epsilon_c\rangle$ and standard deviation σ_r of the detection efficiencies have been computed.

The dependence of the obtained results with the nucleus follows the same trend as the one presented in Fig. 4 for the C_6D_6 detectors. For this reason, we show in Fig. 10 the distribution of the $\langle\epsilon_c\rangle$ and σ_r values instead, for different m_{cr} cuts. As expected, when the detection efficiencies are high (*All* m_{cr}) then the σ_r are small. However, when the efficiencies decrease, the values of σ_r are distributed over an increasing range.

5. Summary and conclusions

The Pulse Height Weighting Technique (PHWT) is widely used to measure (n, γ) cross sections as a function of the neutron energy. This technique, used with low efficiency γ-ray detectors, is intended to solve the problem that the detection efficiency changes with the neutron energy. The main purpose of this work has been to show how to measure neutron capture cross sections with a high efficiency segmented detector which uses the PHWT.

Such a detector would have, at least, the following advantages over other low efficiency detection systems: (i) reduce the uncertainty due to counting statistics, (ii) be less sensitive to anisotropic emission or to angular correlations of the measured capture γ-rays, and (iii) in the case of not using the PHWT in the data analysis, i.e. not using weights, it would allow to impose conditions on the detected events to improve the capture to background ratio.

In this paper we have first described how the PHWT can be extended from one to several detectors. Then, we have used NuDEX and Geant4 to simulate the response of three C_6D_6 detection systems (with a small, intermediate and high detection efficiencies) to more than 20.000 different (n, γ) cascades. We have used the obtained results to quantify how the capture detection efficiency (ϵ_c) and the equivalent variable when using the PHWT (ξ_c^w), vary with the neutron energy.

The results show that, according to the predictions of the (n, γ) cascade generation model used, the variations of ξ_c^w are less than 2% in almost all the nuclei tested (~200). These results thus validate the PHWT for these detection systems for realistic cascades, taking into account effects such as the electron conversion and the energy threshold of the detectors.

After that, we have studied the effect of using weights in the statistical fluctuations when performing measurements with the PHWT. These fluctuations are larger than when no weights are used. We have obtained that, when the number of capture reactions detected is large, using the PHWT has an effect on the statistical fluctuations equivalent to reducing the capture detection efficiency by $\sim 1.8 - 3.5$, depending on the nucleus and on the experimental setup.

From all these simulation, we have also obtained that for a large number of nuclei the capture detection efficiency ϵ_c does not seem to change significantly with the neutron energy. This may allow to perform measurements without the PHWT with experimental setups which usually apply the PHWT. This has the advantage of both reducing the statistical fluctuations and being able to impose conditions on the detected events to improve the capture to background ratio.

Finally, we have made use of this methodology to carry out a similar study with the n_TOF TAC. The obtained results allow to quantify the variations in the capture detection efficiency, depending on the measured nucleus and on the conditions imposed on the detected events to discriminate capture from background.

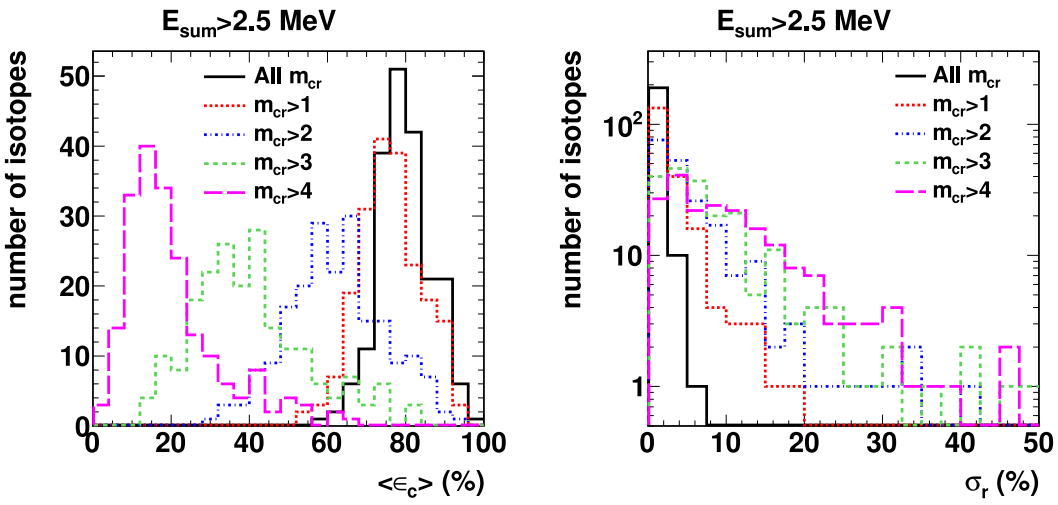

Fig. 10. Distribution of the mean values ($\langle\epsilon_c\rangle$, left) and standard deviations (σ_r, right) of the capture detection efficiencies in the n_TOF TAC obtained after simulating capture cascades of ∼ 200 different nuclei, with 100 sub-realizations of each. The efficiencies have been computed for detected events with total deposited energy larger than 2.5 MeV ($E_{sum} > 2.5$ MeV) and different conditions in the crystal multiplicity (m_{cr}).

Declaration of competing interest

The authors declare that they have no known competing financial interests or personal relationships that could have appeared to influence the work reported in this paper.

Data availability

Data will be made available on request.

Acknowledgments

This work was supported in part by the I+D+i grant PGC2018-096717-B-C21 funded by MCIN/AEI/10.13039/501100011033 and by the European Commission H2020 Framework Programme project SANDA (Grant agreement ID: 847552).

References

[1] A. Bensussan, J. Salome, Nucl. Instrum. Methods A 155 (1) (1978) 11–23, http://dx.doi.org/10.1016/0029-554X(78)90181-7.
[2] P.W. Lisowski, C.D. Bowman, G.J. Russell, S.A. Wender, Nucl. Sci. Eng. 106 (2) (1990) 208–218, http://dx.doi.org/10.13182/NSE90-A27471.
[3] C. Guerrero, et al., the n_TOF Collaboration Collaboration, Eur. Phys. J. A 49 (2) (2013) 1–15, http://dx.doi.org/10.1140/epja/i2013-13027-6.
[4] X. Ledoux, et al., Radiat. Prot. Dosim. 180 (1–4) (2017) 115–119, http://dx.doi.org/10.1093/rpd/ncx257.
[5] J. Tang, et al., Nucl. Sci. Tech. 32 (2021) 11, http://dx.doi.org/10.1007/s41365-021-00846-6.
[6] C. Domingo-Pardo, et al., the n_TOF Collaboration Collaboration, J. Phys.: Conf. Ser. 1668 (2020) 012013, http://dx.doi.org/10.1088/1742-6596/1668/1/012013.
[7] V. Alcayne, et al., the n_TOF Collaboration Collaboration, EPJ Web Conf. 211 (2019) 03008, http://dx.doi.org/10.1051/epjconf/201921103008.
[8] E. Mendoza, et al., the n_TOF Collaboration Collaboration, Phys. Rev. C 97 (2018) 054616, http://dx.doi.org/10.1103/PhysRevC.97.054616.
[9] V. Alcayne, Measurement of the Cm-244, Cm-246 and Cm-248 neutron-induced capture cross sections at the CERN n_TOF facility, (Ph.D. thesis), Universidad Complutense de Madrid, 2022, https://cds.cern.ch/record/2811791.
[10] T. Gozani, R. Ginaven, Nucl. Instrum. Methods 76 (2) (1969) 333–336, http://dx.doi.org/10.1016/0029-554X(69)90037-8.
[11] C. Guerrero, et al., the n_TOF Collaboration Collaboration, Phys. Rev. Lett. 125 (2020) 142701, http://dx.doi.org/10.1103/PhysRevLett.125.142701.
[12] R. Plag, M. Heil, F. Käppeler, P. Pavlopoulos, R. Reifarth, K. Wisshak, Nucl. Instrum. Methods A 496 (2) (2003) 425–436, http://dx.doi.org/10.1016/S0168-9002(02)01749-7.
[13] C. Massimi, et al., the n_TOF Collaboration Collaboration, Phys. Rev. C 85 (2012) 044615, http://dx.doi.org/10.1103/PhysRevC.85.044615.
[14] M.Q. Buckner, C.Y. Wu, R.A. Henderson, B. Bucher, N. Wimer, A. Chyzh, T.A. Bredeweg, B. Baramsai, A. Couture, M. Jandel, S. Mosby, J.L. Ullmann, Phys. Rev. C 95 (2017) 061602, http://dx.doi.org/10.1103/PhysRevC.95.061602.
[15] J. Lerendegui-Marco, et al., the n_TOF Collaboration Collaboration, Phys. Rev. C 97 (2018) 024605, http://dx.doi.org/10.1103/PhysRevC.97.024605.
[16] C. Domingo-Pardo, et al., the n_TOF Collaboration Collaboration, Phys. Rev. C 76 (2007) 045805, http://dx.doi.org/10.1103/PhysRevC.76.045805.
[17] G. Tagliente, et al., the n_TOF Collaboration Collaboration, Phys. Rev. C 87 (2013) 014622, http://dx.doi.org/10.1103/PhysRevC.87.014622.
[18] P.S. S. Kopecky, A. Moens, Low energy transmission measurements of ^{240,242}Pu at GELINA and their impact on the capture width, International Conference on Nuclear Data for Science and Technology, Berlin, Heidelberg, 2008, pp. 623–626, http://dx.doi.org/10.1051/ndata:07391.
[19] N. Bohr, Nature 137 (1936) 344–348, http://dx.doi.org/10.1038/137344a0.
[20] N. Bohr, J.A. Wheeler, Phys. Rev. 56 (1939) 426–450, http://dx.doi.org/10.1103/PhysRev.56.426.
[21] M. Moxon, E. Rae, Nucl. Instrum. Methods 24 (1963) 445–455, http://dx.doi.org/10.1016/0029-554X(63)90364-1.
[22] R.L. Macklin, J.H. Gibbons, Phys. Rev. 159 (1967) 1007–1012, http://dx.doi.org/10.1103/PhysRev.159.1007.
[23] F. Corvi, F. Gunsing, C. Bastian, A. Brusegan, N. Herault, J. Gonzalez, V. Gressier, A. Lepretre, E. Macavero, C. Mounber, G. Noguere, C. Raepsaet, P. Siegler, J. Nucl. Sci. Technol. 39 (sup2) (2002) 1067–1072, http://dx.doi.org/10.1080/00223131.2002.10875286.
[24] K.H. Guber, L.C. Leal, R.O. Sayer, P.E. Koehler, T.E. Valentine, H. Derrien, J.A. Harvey, AIP Conf. Proc. 769 (1) (2005) 1706–1711, http://dx.doi.org/10.1063/1.1945338.
[25] A. Kimura, et al., Eur. Phys. J. A 51 (2015) 180, http://dx.doi.org/10.1140/epja/i2015-15180-2.
[26] E. Chiaveri, et al., the n_TOF Collaboration Collaboration, EPJ Web Conf. 239 (2020) 17001, http://dx.doi.org/10.1051/epjconf/202023917001.
[27] B. Jiang, J. Han, J. Ren, W. Jiang, X. Wang, Z. Guo, J. Zhang, J. Hu, J. Chen, X. Cai, H. Wang, L. Liu, X. Li, X. Hu, Y. Zhang, Chin. Phys. B 31 (6) (2022) 060101, http://dx.doi.org/10.1088/1674-1056/ac5394.
[28] C. Guerrero, et al., Nucl. Instrum. Methods A 608 (3) (2009) 424–433, http://dx.doi.org/10.1016/j.nima.2009.07.025.
[29] R. Macklin, J. Gibbons, T. Inada, Nuclear Phys. 43 (1963) 353–362, http://dx.doi.org/10.1016/0029-5582(63)90356-0.
[30] G. Walter, H. Beer, F. Kaeppeler, G. Reffo, F. Fabbri, Astron. Astrophys. 167 (1) (1986) 186–199.
[31] P.E. Koehler, R.R. Spencer, R.R. Winters, K.H. Guber, J.A. Harvey, N.W. Hill, M.S. Smith, Phys. Rev. C 54 (1996) 1463–1477, http://dx.doi.org/10.1103/PhysRevC.54.1463.
[32] S. Mizuno, M. Igashira, K. Masuda, Nucl. Sci. Tech. 36 (6) (1999) 493–507, http://dx.doi.org/10.1080/18811248.1999.9726232.
[33] U. Abbondanno, et al., the n_TOF Collaboration Collaboration, Nucl. Instrum. Methods A 521 (2) (2004) 454–467, http://dx.doi.org/10.1016/j.nima.2003.09.066.
[34] F. Perey, J. Johnson, T. Gabriel, R. Macklin, R. Winters, J. Todd, N. Hill, Nuclear Data for Science and Technology, Milto, Japan, 1988, p. 379.
[35] F. Corvi, A. Prevignano, H. Liskien, P. Smith, Nucl. Instrum. Methods A 265 (3) (1988) 475–484, http://dx.doi.org/10.1016/S0168-9002(98)90016-X.

[36] F. Corvi, G. Fioni, F. Gasperini, P.B. Smith, Nucl. Sci. Eng. 107 (3) (1991) 272–283, http://dx.doi.org/10.13182/NSE91-A23790.
[37] J. Tain, et al., J. Nucl. Sci. Technol. 39 (2002) 689–692, http://dx.doi.org/10.1080/00223131.2002.10875193.
[38] J. Lerendegui, Neutron radiative capture on Pu-242: addressing the target accuracies for innovative nuclear systems, (Ph.D. thesis), Universidad de Sevilla, 2018, https://cds.cern.ch/record/2661485.
[39] P.A. PZyla, R.M. Barnett, et al., Prog. Theor. Exp. Phys. 2020 (8) (2020) http://dx.doi.org/10.1093/ptep/ptaa104, 083C01.
[40] F. James, Statistical Methods in Experimental Physics, World Scientific, Singapore, 2006.
[41] P.R. Bevington, D.K. Robinson, Data Reduction and Error Analysis for the Physical Sciences; 3rd Ed., McGraw-Hill, New York, NY, 2003.
[42] J.F. Briesmeister, MCNP: A General Monte Carlo N-Particle Transport Code, Technical Report, LA-13709-M, 2000.
[43] S. Agostinelli, et al., the GEANT4 Collaboration Collaboration, Nucl. Instrum. Methods A 506 (3) (2003) 250–303, http://dx.doi.org/10.1016/S0168-9002(03)01368-8.
[44] J. Allison, et al., Nucl. Instrum. Methods A 835 (2016) 186–225, http://dx.doi.org/10.1016/j.nima.2016.06.125.
[45] E. Mendoza, D. Cano-Ott, D. Jordan, J. Tain, A. Algora, EPJ Web Conf. 239 (2020) 17006, http://dx.doi.org/10.1051/epjconf/202023917006.
[46] E. Mendoza, et al., the n_TOF Collaboration Collaboration, EPJ Web Conf. 239 (2020) 01015, http://dx.doi.org/10.1051/epjconf/202023901015.
[47] F. Bečvář, Nucl. Instrum. Methods A 417 (2) (1998) 434–449, http://dx.doi.org/10.1016/S0168-9002(98)00787-6.
[48] D. Jordan, A. Algora, J. Tain, Nucl. Instrum. Methods A 828 (2016) 52–57, http://dx.doi.org/10.1016/j.nima.2016.05.034.
[49] R. Capote, et al., Nucl. Data Sheets 110 (12) (2009) 3107–3214, http://dx.doi.org/10.1016/j.nds.2009.10.004.
[50] M.R. Bhat, in: S.M. Qaim (Ed.), Nuclear Data for Science and Technology, Springer Berlin Heidelberg, Berlin, Heidelberg, 1992, pp. 817–821, http://dx.doi.org/10.1007/978-3-642-58113-7_227.
[51] I. Band, M. Trzhaskovskaya, C. Nestor, P. Tikkanen, S. Raman, At. Data Nucl. Data Tables 81 (1) (2002) 1–334, http://dx.doi.org/10.1006/adnd.2002.0884.
[52] S. Goriely, et al., Eur. Phys. J. A 55 (2019) 172, http://dx.doi.org/10.1140/epja/i2019-12840-1.
[53] S. Valenta, et al., Phys. Rev. C 96 (2017) 054315, http://dx.doi.org/10.1103/PhysRevC.96.054315.
[54] K. Kobayashi, S. Lee, S. Yamamoto, H.J. Cho, Y. Fujita, J. Nucl. Sci. Technol. 39 (2) (2002) 111–119, http://dx.doi.org/10.1080/18811248.2002.9715164.
[55] B.C. Diven, J. Terrell, A. Hemmendinger, Phys. Rev. 120 (1960) 556–569, http://dx.doi.org/10.1103/PhysRev.120.556.
[56] G.V. Muradyan, Y.V. Adamchuk, Y.G. Shchepkin, M.A. Voskanyan, Nucl. Sci. Eng. 90 (1) (1985) 60–74, http://dx.doi.org/10.13182/NSE85-A17431.
[57] D.P. Barry, M.J. Trbovich, Y. Danon, R.C. Block, R.E. Slovacek, G. Leinweber, J.A. Burke, N.J. Drindak, Nucl. Sci. Eng. 153 (1) (2006) 8–25, http://dx.doi.org/10.13182/NSE06-A2590.
[58] K. Wisshak, K. Guber, F. Käppeler, J. Krisch, H. Müller, G. Rupp, F. Voss, Nucl. Instrum. Methods A 292 (3) (1990) 595–618, http://dx.doi.org/10.1016/0168-9002(90)90179-A.
[59] S. Yamamoto, K. Kobayashi, Y. Fujita, J. Nucl. Sci. Technol. 33 (11) (1996) 815–820, http://dx.doi.org/10.1080/18811248.1996.9732014.
[60] K. Wisshak, F. Voss, F. Käppeler, G. Reffo, Phys. Rev. C 42 (1990) 1731–1750, http://dx.doi.org/10.1103/PhysRevC.42.1731.
[61] R. Reifarth, M. Heil, F. Käppeler, F. Voss, K. Wisshak, F. Becvář, M. Krtička, R. Gallino, Y. Nagai, Phys. Rev. C 66 (2002) 064603, http://dx.doi.org/10.1103/PhysRevC.66.064603.
[62] M. Heil, R. Reifarth, M. Fowler, R. Haight, F. Käppeler, R. Rundberg, E. Seabury, J. Ullmann, J. Wilhelmy, K. Wisshak, Nucl. Instrum. Methods A 459 (1) (2001) 229–246, http://dx.doi.org/10.1016/S0168-9002(00)00993-1.
[63] L. Xie, et al., J. Instrum. 16 (10) (2021) P10029, http://dx.doi.org/10.1088/1748-0221/16/10/p10029.
[64] C. Guerrero, et al., the n_TOF Collaboration Collaboration, Phys. Rev. C 85 (2012) 044616, http://dx.doi.org/10.1103/PhysRevC.85.044616.
[65] E. Mendoza, et al., the n_TOF Collaboration Collaboration, Phys. Rev. C 90 (2014) 034608, http://dx.doi.org/10.1103/PhysRevC.90.034608.
[66] B. Baramsai, et al., Phys. Rev. C 96 (2017) 024619, http://dx.doi.org/10.1103/PhysRevC.96.024619.
[67] M. Jandel, et al., Phys. Rev. C 78 (2008) 034609, http://dx.doi.org/10.1103/PhysRevC.78.034609.
[68] C.J. Prokop, A. Couture, S. Jones, S. Mosby, G. Rusev, J. Ullmann, M. Krtička, Phys. Rev. C 99 (2019) 055809, http://dx.doi.org/10.1103/PhysRevC.99.055809.
[69] M. Weigand, et al., Phys. Rev. C 92 (2015) 045810, http://dx.doi.org/10.1103/PhysRevC.92.045810.
[70] C. Guerrero, D. Cano-Ott, E. Mendoza, J. Taín, A. Algora, E. Berthoumieux, N. Colonna, C. Domingo-Pardo, E. González-Romero, M. Heil, D. Jordán, F. Käppeler, C. Lampoudis, T. Martínez, C. Massimi, R. Plag, Nucl. Instrum. Methods A 671 (2012) 108–117, http://dx.doi.org/10.1016/j.nima.2011.12.046.